

Supplementary Information for

**Fabrication of porous organic polymers in the form of powder,
soluble in organic solvents and nanoparticles: a unique platform for
gas adsorption and efficient chemosensing**

Sujoy Bandyopadhyay, Pragyan Pallavi, Amith G. Anil and Abhijit Patra*

Department of Chemistry, Indian Institute of Science, Education and Research (IISER) Bhopal,
Bhopal-462066, Fax: +91 (0)755 409 2392; Tel: +91 (0)755 669 2378

E-mail: abhijit@iiserb.ac.in

CONTENTS

Pages

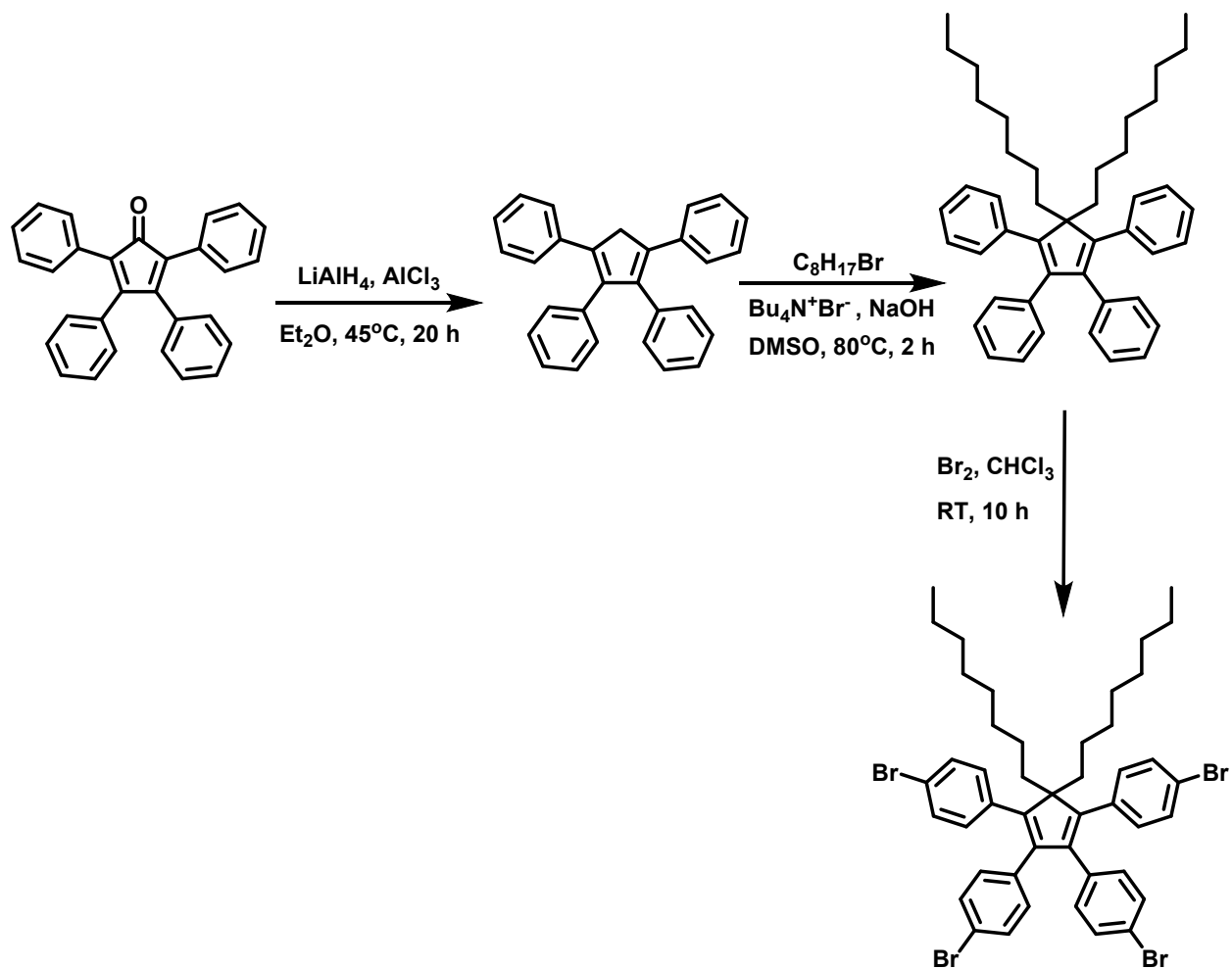
2 – 10	I. Synthesis and Characterization (a) Chemicals, reaction scheme (b) Characterization of polymers
11 – 12	II. Details of morphology and EDX analysis (a) Fabrication of samples (b) EDX analysis
13 – 14	III. Gas sorption Additional sorption isotherms
15 – 17	IV. Atomistic simulation
18 – 21	V. Spectroscopic data (a) Absorption, steady state fluorescence and quantum yield measurements (b) Time resolved fluorescence measurements
22 – 30	VI. Explosive sensing
31	VII. Tunable emission
32	References
33 – 36	^1H, ^{13}C NMR spectra

I. Synthesis and Characterization

Instrumentation: ^1H and ^{13}C -NMR spectra were recorded on Bruker Avance III 500, 700 MHz NMR spectrometers. The chemical shifts (δ) are reported in parts per million (ppm) using residual solvent signals as internal standards. FTIR measurements were carried out on Perkin Elmer FTIR spectrophotometer. Twenty scans were signal-averaged, with a resolution of 8 cm^{-1} at room temperature. KBr pellet was used for the measurements. Molecular weights of the soluble polymers were estimated by Gel Permeation Chromatography (GPC, Polymer Laboratories). THF was used as the eluent with flow rate of 1 mL/min at 40°C and polystyrene was used as the calibration standard. Universal calibration was used employing refractive index and viscometry detectors. Ultrasonication was carried out with Branson sonifier (model: W-450) using microtip of 5 mm tip diameter.

(a) Chemicals: All chemicals were used as received unless stated otherwise. 1,2,3,4-tetraphenyl-1,3-cyclopentadienone (98%), lithium aluminum hydride (95%), aluminum chloride (99.9%) copper(I) iodide (99.995%), bis(triphenylphosphine)palladium(II) dichloride (98%), sodium dodecyl sulfate (99%), dimethyl sulfoxide (99%) toluene (99.85%), diisopropylamine (99%), tetrakis(triphenylphosphine)palladium (99.9%), and 1,4-diethynylbenzene (95%) were received from Sigma-Aldrich. Bromine (99.5%), sodium hydroxide (99%), picric acid (98%), chloroform and hexane were received from Merck. THF (99%), Ethanol (99.8%), extra pure concentrated HCl were received from Spectrochem. 1,4-diethynylbenzene was further purified by washing through a silica gel column and subsequent recrystallizations.

Reaction scheme:



Scheme S1. Synthetic route for the monomer tetrakis(4-bromophenyl)-5,5-dioctylcyclopentadiene (TBDC).

^1H , ^{13}C NMR spectra of all final compounds are provided at the end.

(b) Characterization of polymers

(i) Fourier transform infrared (FTIR) spectroscopy

The FTIR spectrum of **P1** (Fig. S1) shows characteristic band at 2202 cm^{-1} corresponds to $\text{C}\equiv\text{C}$ stretching indicating coupling between tetrakis(4-bromophenyl)-5,5-dioctylcyclopentadiene (TBDC) and 1,4-diethynylbenzene (DEB). The characteristic aliphatic C-H stretching at $2926 - 2852\text{ cm}^{-1}$ originating from TPDC building blocks are also observed. Absorption band at 3037 cm^{-1} is assigned to $\text{C}_{\text{Ar}}\text{-H}$ stretching. Aromatic ring (C=C) stretching bands are observed at 1596 and 1489 cm^{-1} . Strong band in the region of 829 cm^{-1} can be attributed to C-H bending of para-di-substituted benzene ring. Comparison of FTIR spectrum of **P1** with that of constituent monomers and with that of **P2** and **P3** are shown in Fig. S2 and S3 respectively.

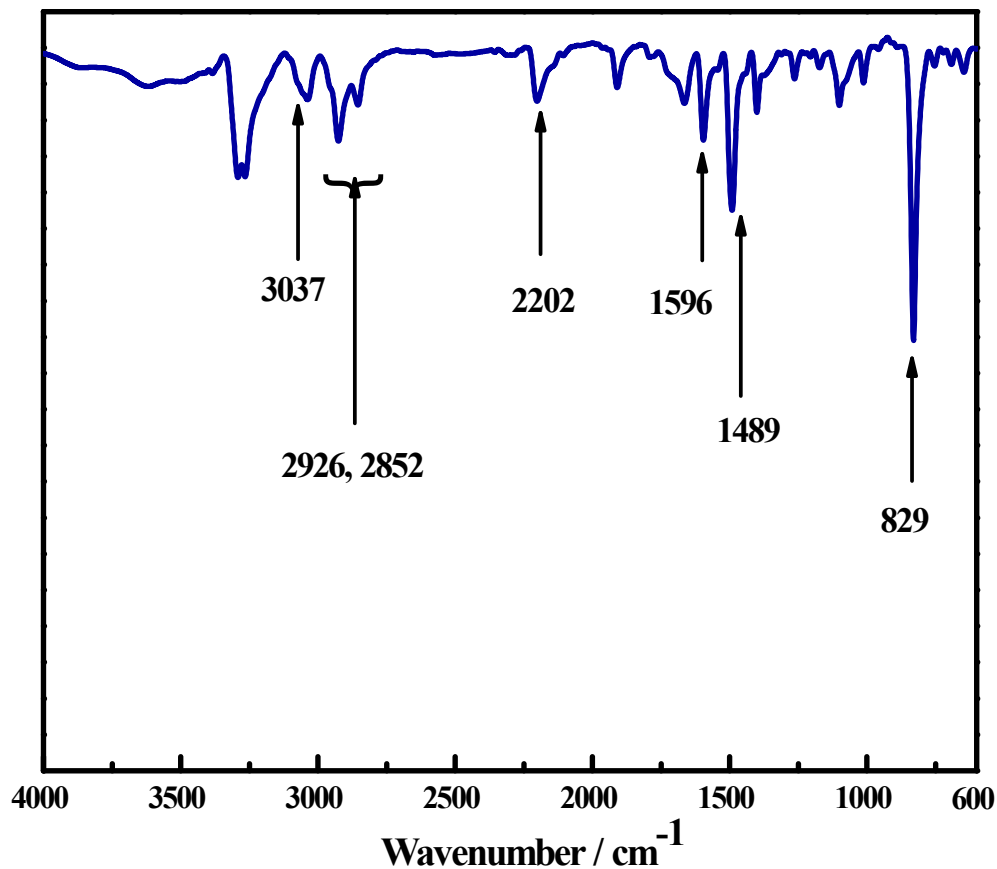


Fig. S1. FTIR spectrum of **P1**.

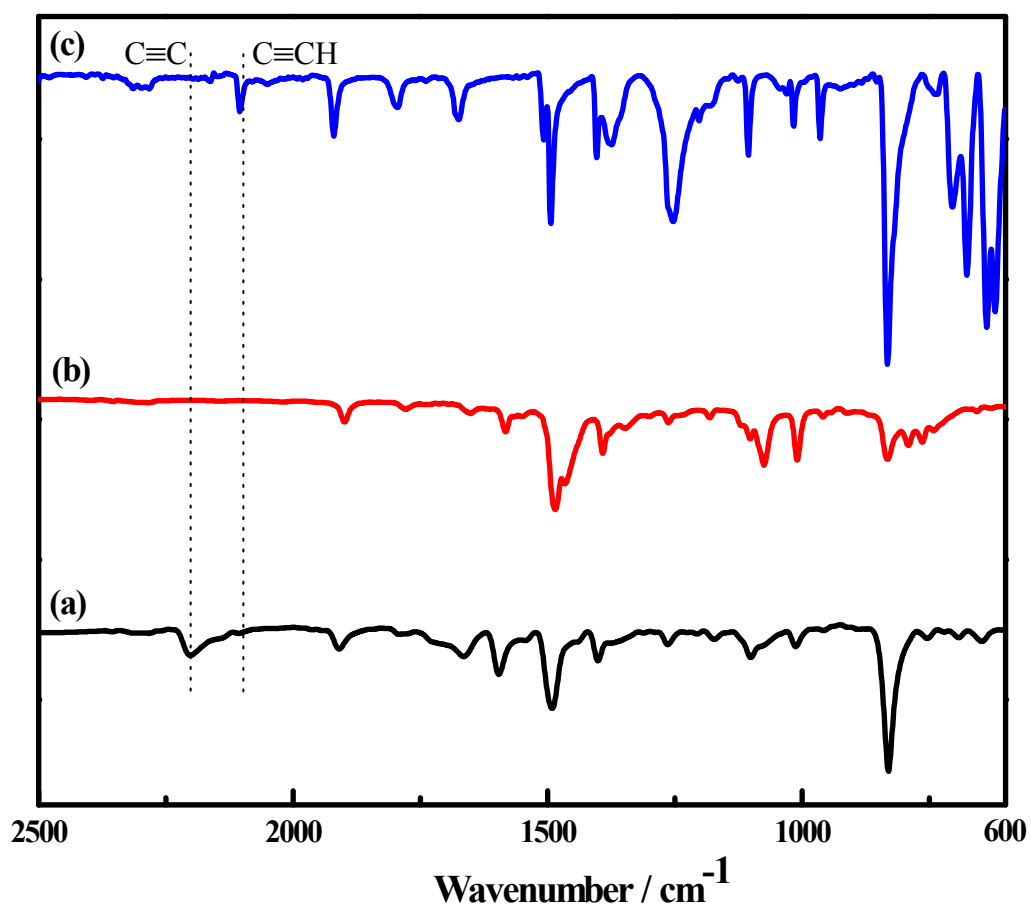


Fig. S2. FTIR spectra of (a) P1, (b) TBDC and (c) DEB.

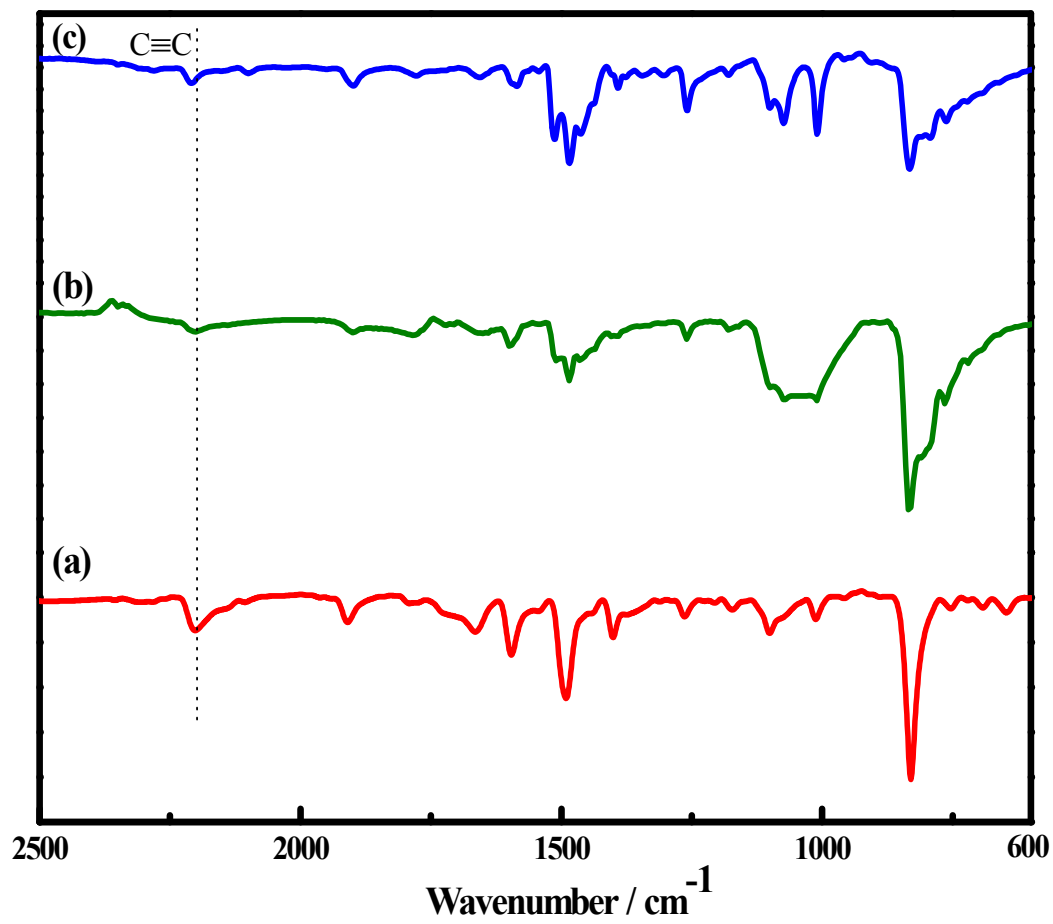


Fig. S3. FTIR spectra of (a) P1, (b) P2 and (c) P3.

(ii) NMR spectroscopy

^1H NMR and ^{13}C NMR spectra of **P2** and **P3** were recorded in CDCl_3 . Comparison of ^1H NMR spectrum of **P2** with that of constituent monomers clearly indicates similar resonances in addition to other resonances, thus demonstrating polycondensation between the monomers (Fig. S4). Comparison of ^1H NMR spectra of **P2** and **P3** signify that both the polymer have similar repeating unit (Fig. S5). The signal at 89 ppm in ^{13}C NMR spectra of **P2** and **P3** further confirms the presence of $\text{Ar-C}\equiv\text{C-Ar}$ (Fig. S6).

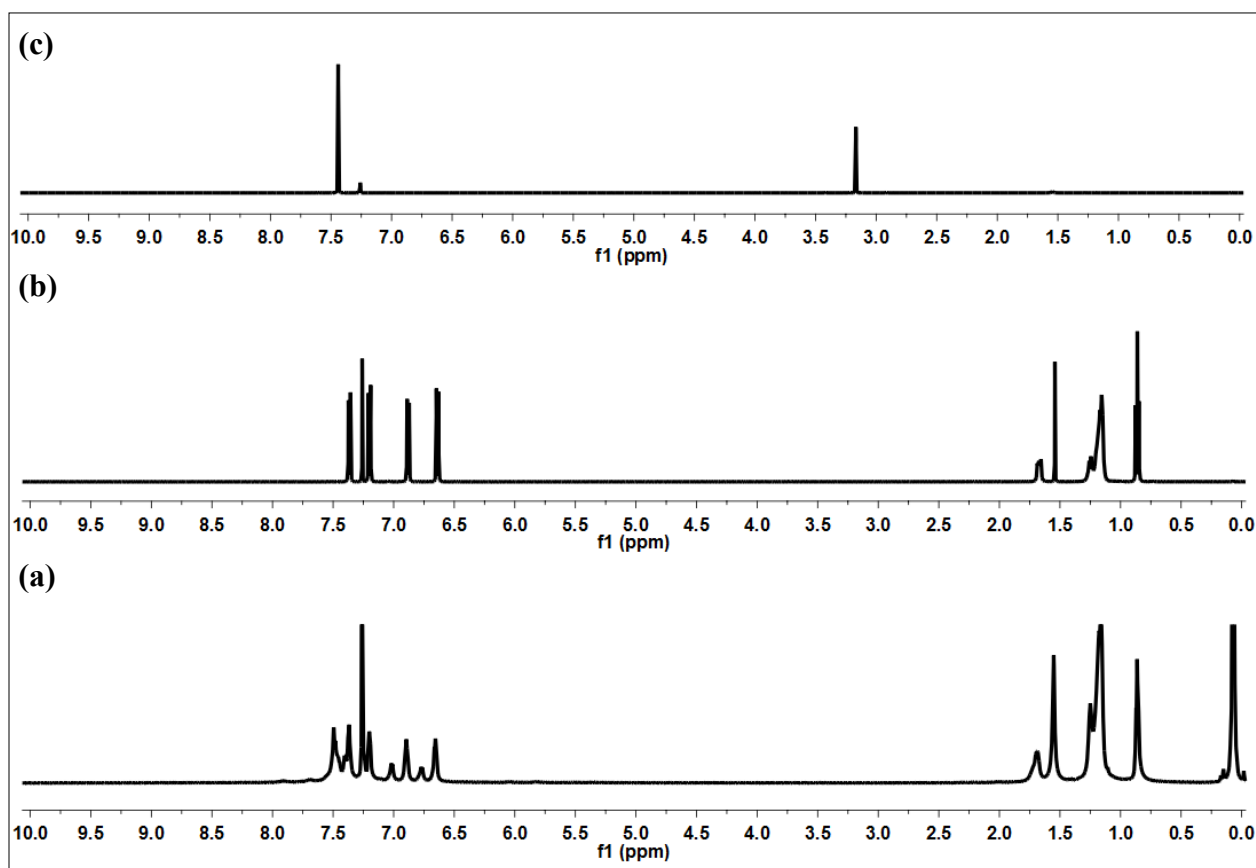


Fig. S4. ^1H NMR spectra of (a) **P2**, (b) **TBDC** and (c) **DEB**.

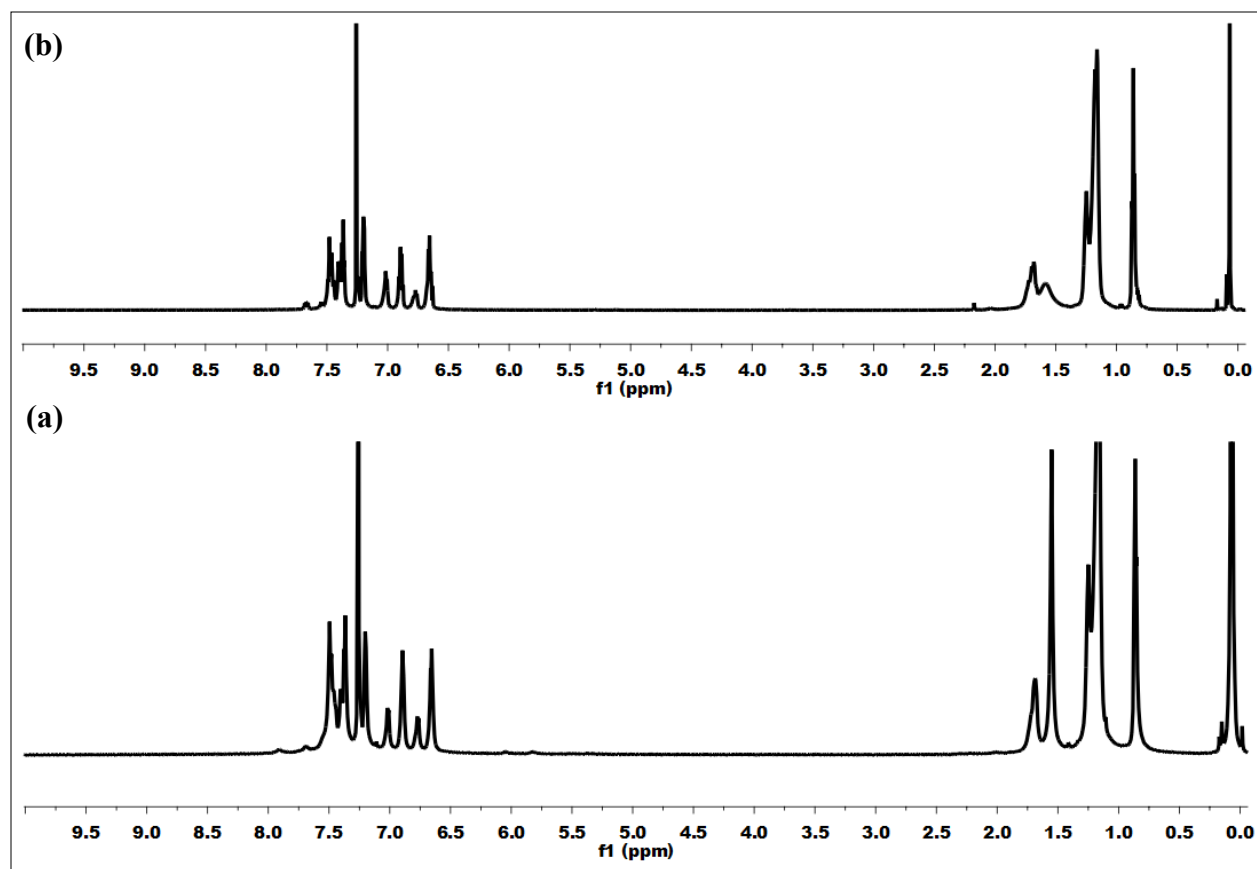


Fig. S5. ^1H NMR spectra of (a) P2 and (b) P3.

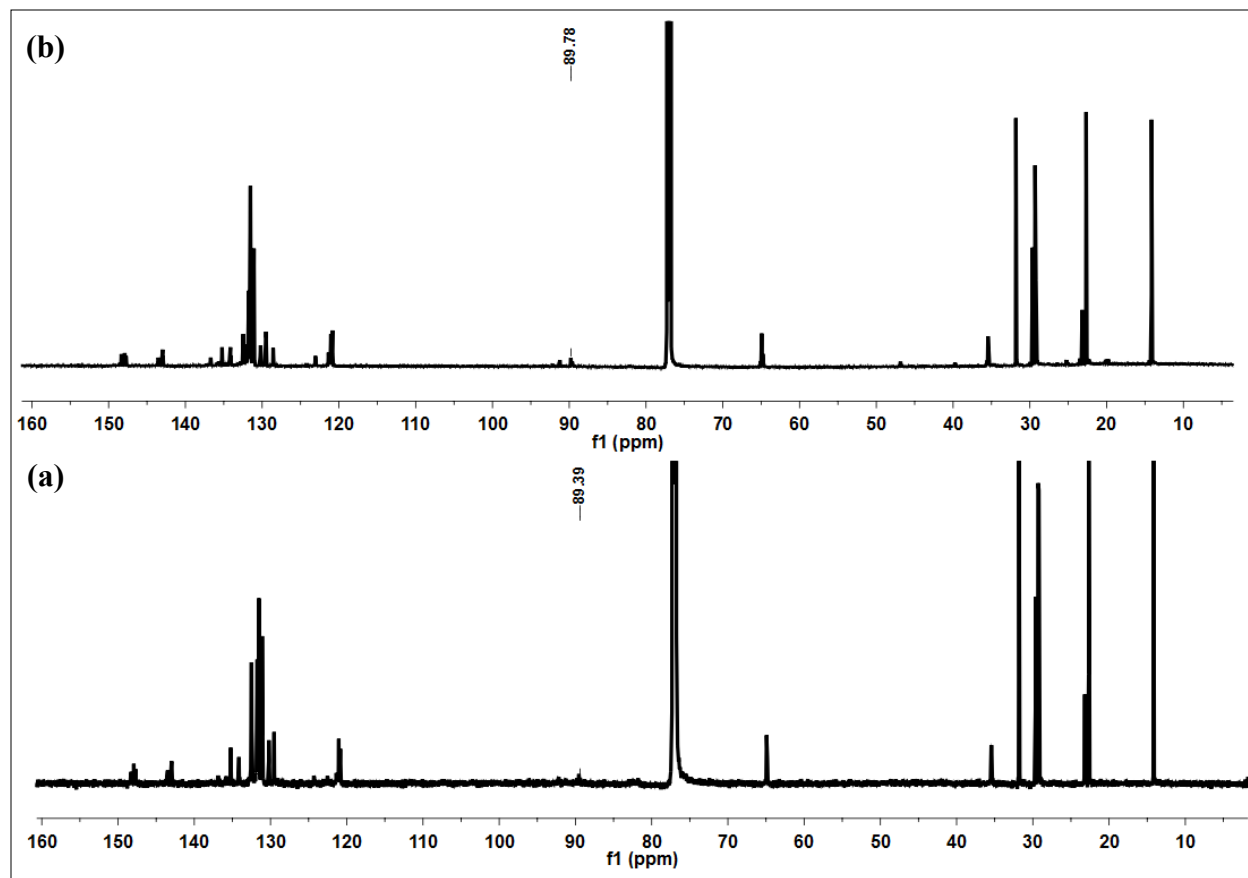


Fig. S6. ^{13}C NMR spectra of (a) **P2** and (b) **P3**.

(iii) Thermogravimetric analysis

Thermogravimetric analysis (TGA) was carried out using Perkin Elmer TGA-6000 instrument. The samples were heated at a rate of $10^{\circ}\text{C min}^{-1}$ under a nitrogen atmosphere to a maximum of 900°C . TGA showed that all the polymers are thermally stable without decomposing up to 375°C (Fig. S7).

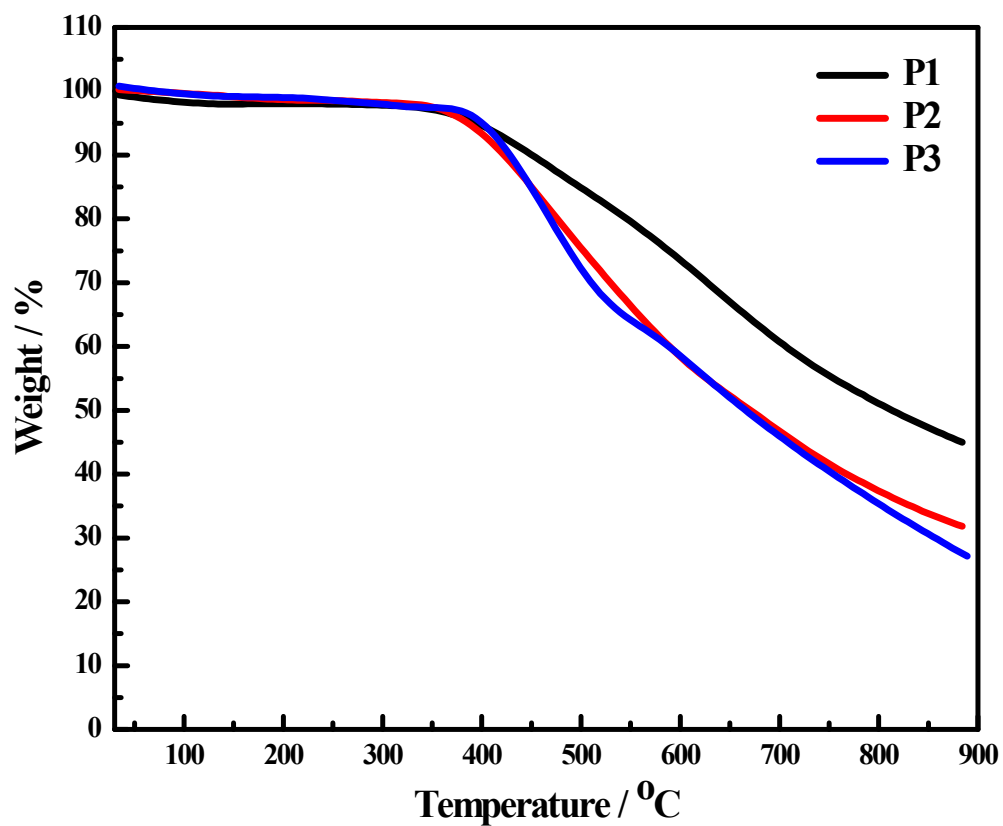


Fig. S7. Thermogravimetric analysis curves of P1, P2 and P3.

II. Details of morphology and EDX analysis

Instrumentation: The surface morphology of all polymers and size of the nanoparticles were examined using Carl Zeiss (Ultraplus) field emission scanning electron microscope (FESEM). Energy dispersive X-ray spectroscopy was examined using a spectrometer (Oxford Instruments X-Max^N) attached to FESEM. Dynamic light scattering (DLS) measurements of aqueous dispersion of nanoparticles (**P3**) were carried out with Beckman Coulter Delso Nano C DLS set up.

(a) Sample preparation for FESEM: Samples for microscopy were prepared by sprinkling (~ 2 mg) powdered polymers on aluminum stub using an adhesive carbon tape. Samples for polymer nanoparticles (**P3**) were prepared by depositing colloidal solution on silicon wafer by drop casting. All samples were coated with a thin layer of sputtered gold prior to imaging. FESEM was carried out using an accelerating voltage of 5 kV and 10 kV.

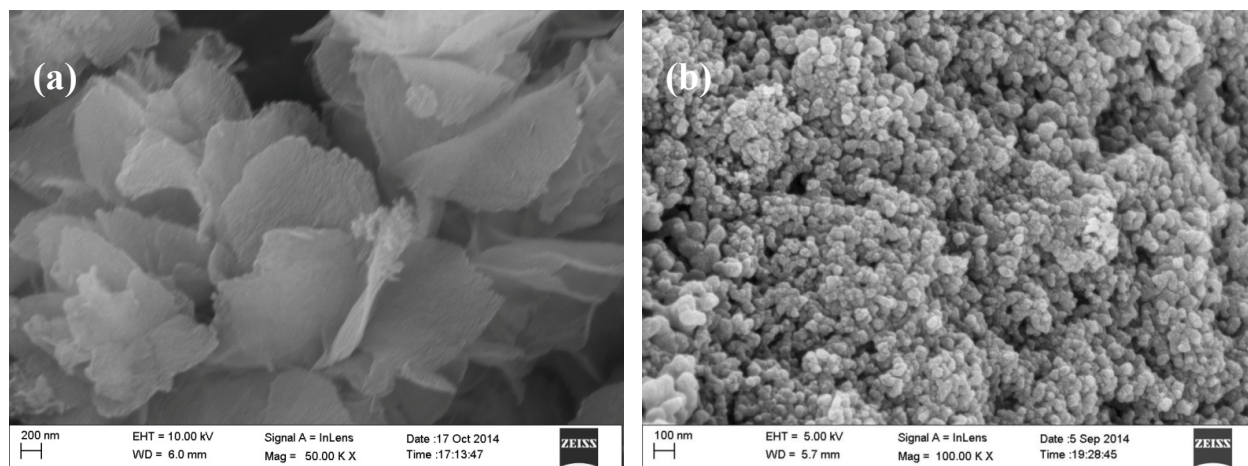


Fig. S8. FESEM images of (a) **P1** and (b) **P2**.

(b) EDX analysis

The EDX was performed at a working voltage of 30 kV and was standardized with Co element.

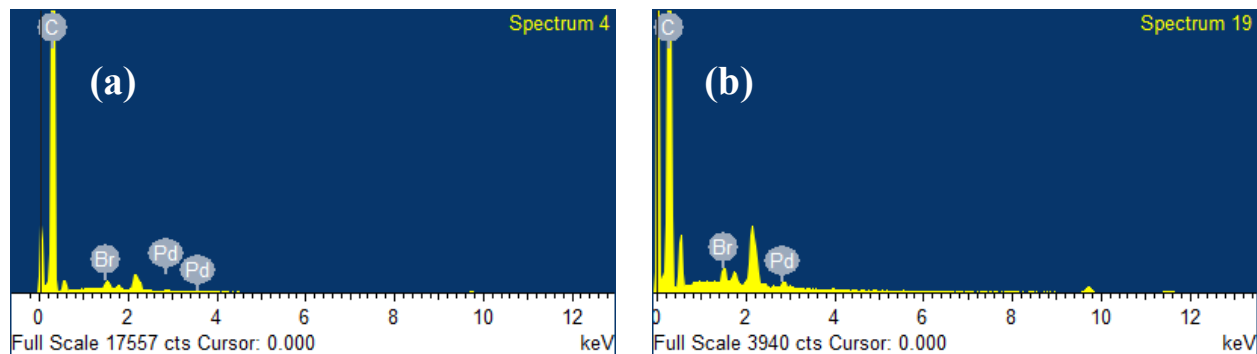


Fig. S9. EDX profile of (a) P1 and (b) P2.

Table S1. Atomic and weight percentages of carbon, bromine and palladium obtained from EDX analysis.

Sample		Carbon	Bromine	Palladium
P1	Weight %	98.74	0.74	0.53
	Atomic %	99.83	0.11	0.06
P2	Weight %	98.51	1.07	0.42
	Atomic %	99.79	0.16	0.05

III. Gas sorption

Instrumentation: All gas adsorption experiments were performed on a Quantachrome Autosorb QUA211011 equipment. Nitrogen adsorption isotherms were analyzed using ASIQwin software.

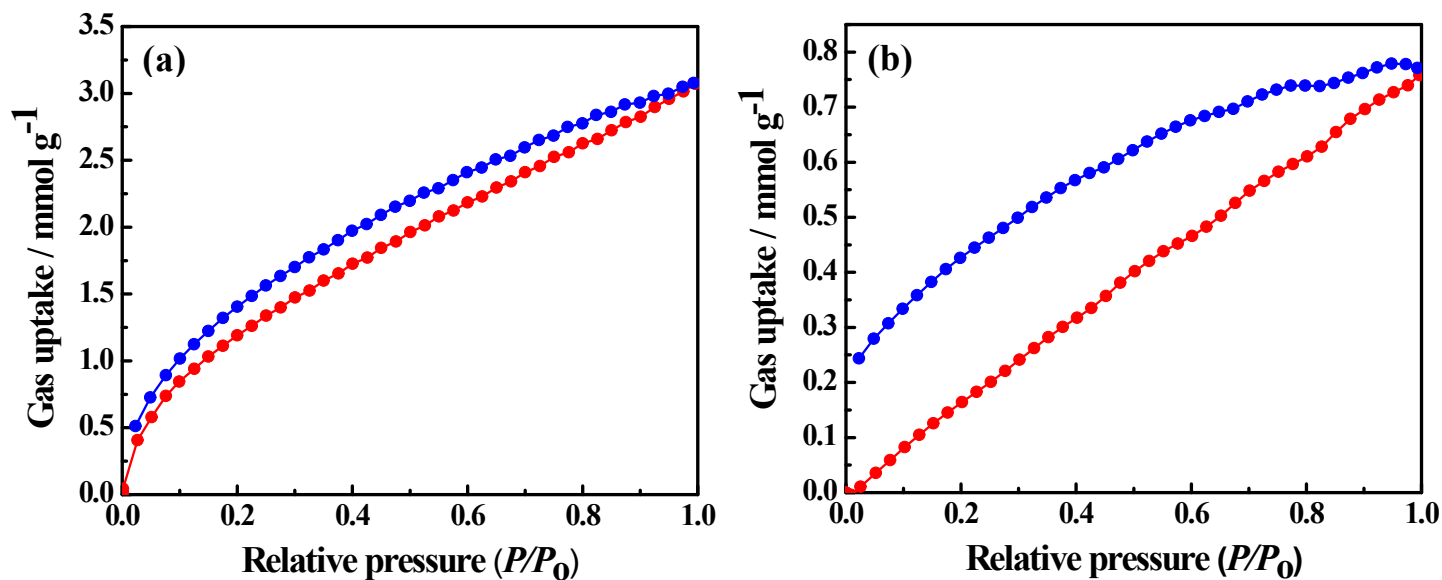


Fig. S10. Gas sorption isotherms of **P1** for (a) hydrogen at 77 K and (b) carbon dioxide at 298 K (red circles: adsorption, blue circles: desorption).

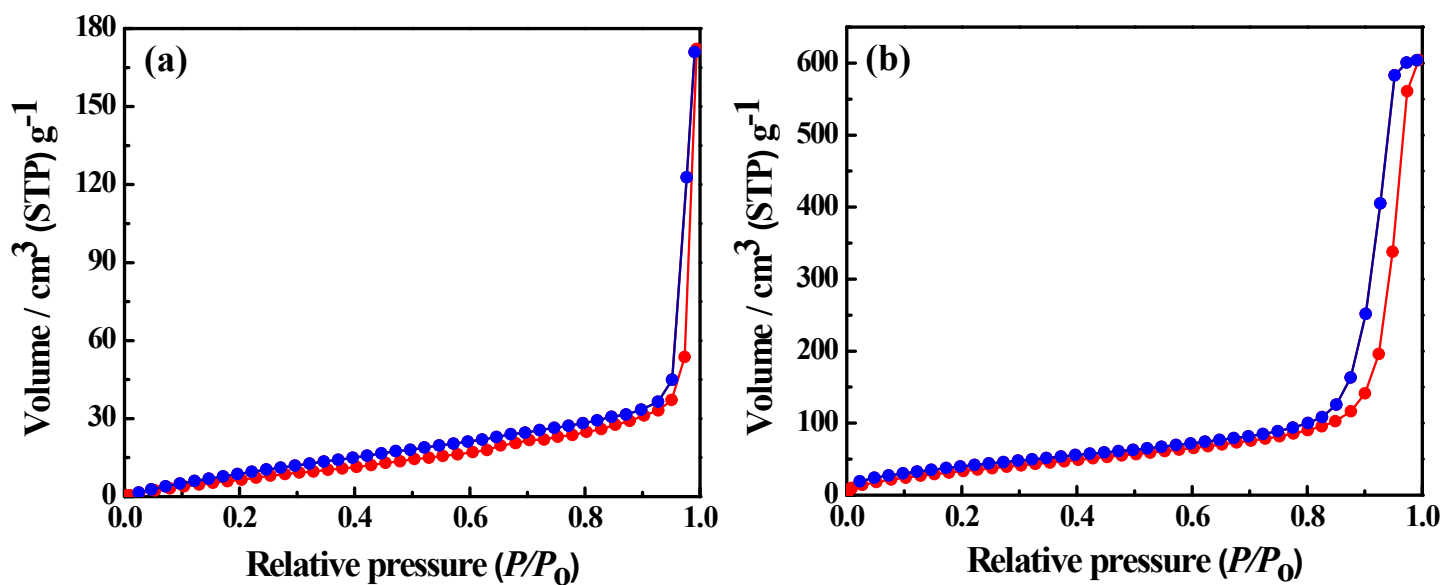


Fig. S11. Nitrogen sorption isotherms of (a) **P2** and (b) **P3** at 77 K (red circles: adsorption, blue circles: desorption).

Table S2. Properties of porous networks.

Sample	$S_{\text{BET}} / \text{m}^2 \text{g}^{-1}$	$V_{0.1} / \text{cm}^3 \text{g}^{-1}$^[a]	$V_{\text{tot}} / \text{cm}^3 \text{g}^{-1}$^[b]
P1	405	0.14	0.68
P2	39	0.0068	0.26
P3	143	0.037	0.93

^[a]Pore volume at $P/P_0 = 0.10$, ^[b]Pore volume at $P/P_0 = 0.99$.

IV. Atomistic Simulation

In order to have visualization of network structure and to understand the structural properties associated with porous nature of TPDC based POPs like pore structure, pore dimension, surface area and gas adsorption, molecular model was built with tetrakis-(4-bromophenyl)-5,5-dioctylcyclopentadiene and 1,4-diethynylbenzene units.¹

Structure generation: Molecular model of TPDC based polymers was built using Materials Studio 6.1 package (*accelrys*). The model structure of polymer was constructed with net molar mass of 16358 g/mol. Energy minimization was done in Discover module using COMPASS forcefield.^{2,3} Optimized model structure of TPDC polymer was packed at low density (0.5 g/cm³) in an amorphous cell with periodic boundary condition.⁴

Molecular dynamics (MD) simulations: All MD simulations were performed using Discover module with smart algorithm in Materials Studio with time step of 1 fs.⁴ Compression and decompression protocol of 21 steps of molecular dynamics was performed to equilibrate the cell.⁶ The Noose Hover thermostat during NVT steps and Andersen barostat were used at NPT steps. The final density of relaxed structure was 0.85 g/cm³. The geometrical surface area calculated from solvent accessible surfaces was found to be 345 m²/g using probe radius of 1.86 Å (kinetic radius of nitrogen) with fine grid resolution.^{5,6} Simulated pore volume was found to be 0.45 cm³/g (Fig. S12). As noted in the main text, BET surface area and pore volume of **P1** obtained from the analysis of N₂ sorption isotherm were found to be 405 m²/g and 0.68 cm³/g. The underestimation of pore volume compared to the experimental result is probably due to the lesser degree of cross linking carried out to built the polymer model, which resulted into the flexible polymer chains thus preventing the formation of pores.¹

Grand canonical Monte Carlo simulations: The adsorption isotherm of nitrogen was simulated at 77 K up to 1 bar using GCMC simulation.^{3,4} The nitrogen uptake increases sharply at low pressure then attains plateau at higher pressure as analogous to the experimental results (Fig. S13).

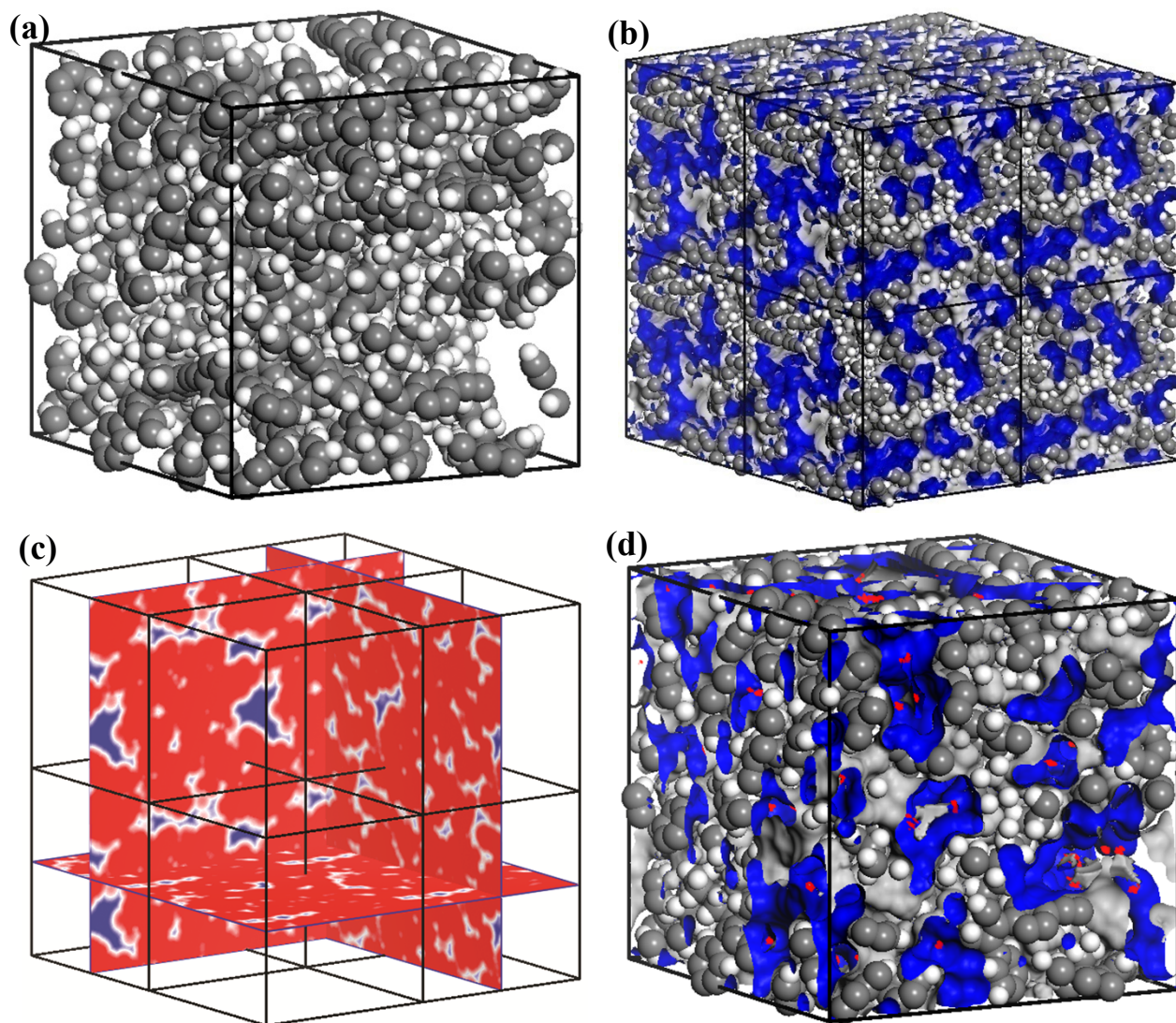


Fig. S12. Snapshots of simulated amorphous cell of TPDC polymer: (a) amorphous cell with periodic boundary conditions; (b) geometrical surfaces are shown in blue and gray; (c) 3-dimensional 'slices' through simulated pore structure (occupied and unoccupied volumes are shown in red and blue respectively); (d) snapshot of nitrogen sorption in simulated pores at 1 bar and 77 K (red dot: field density of nitrogen) [Cell dimension is about 3.13 nm].

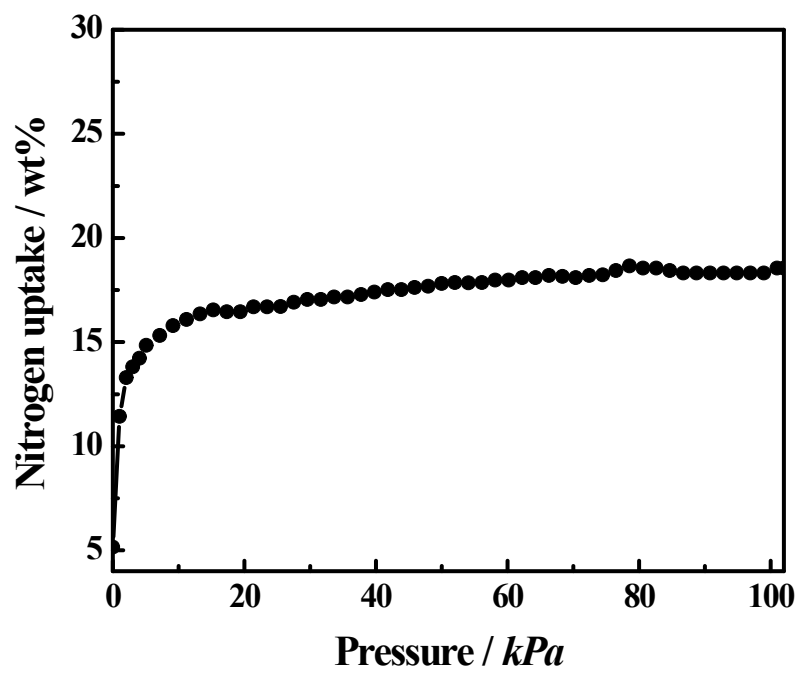


Fig. S13. Simulated nitrogen adsorption isotherm of TPDC based POPs at 77 K at 1 bar.

V. Spectroscopic data

Instrumentation: UV-vis absorption spectra were recorded on a Cary 100 spectrophotometer. Steady state fluorescence measurements were carried out on a Jobin Yvon Horiba Model Fluorolog-3-21.

(a) Steady state spectroscopy

Absorption spectroscopy: Absorption spectra for soluble polymer (**P2**) were recorded in THF and for nanoparticles (**P3**) in ultra pure water (Millipore MilliQ, resistivity = 18 MΩ cm). It was ensured that the optical density is low enough to avoid artifacts due to inner-filter effects. The absorption maxima for THF solution of **P2** and aqueous dispersion of **P3** were found to be at 365 and 340 nm respectively.

Steady state fluorescence spectroscopy: Emission of **P2** and **P3** were investigated by exciting at different wavelengths. Emission for both was found to be excitation wavelength independent. Emission maxima for **P2** in THF and aqueous dispersion of **P3** are 465 and 470 nm respectively. The difference of fluorescent intensity with the excitation wave length is due to the difference in optical densities at those wavelengths.

Fluorescence quantum yield (Φ_f) measurement: The fluorescence quantum yields of **P2** in THF and **P3** in water were estimated by comparison with coumarin-102 in ethanol ($\Phi_f = 0.76$).⁷ The quantum yields were calculated using the following equation.⁸

$$\Phi_{f, x} = \Phi_{f, s} \cdot \frac{F_x}{F_s} \cdot \frac{f_s}{f_x} \cdot \frac{n_x^2}{n_s^2}$$

where, Φ_f is fluorescence quantum yield, subscript x denotes unknown sample and subscript s refers to standard. F denotes integral fluorescence, n refers to refractive index of the solvent used in the measurements and f is the absorption factor at the excitation wavelength given by the following equation:

$f = 1 - 10^{-\varepsilon(\lambda_{ex})cl} = 1 - 10^{-A(\lambda_{ex})}$, where A is absorbance and ε = molar extinction coefficient in L mol⁻¹ cm⁻¹.

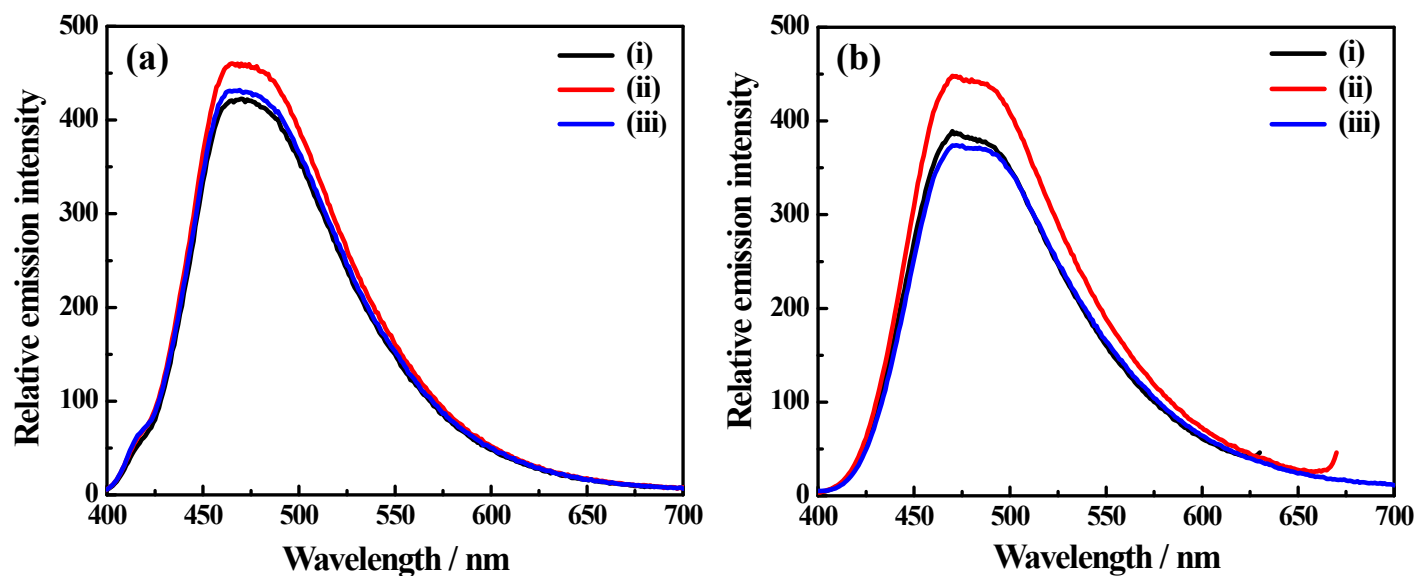


Fig. S14. (a) Emission spectra at different excitation wavelengths for: (a) **P2** in THF (i) $\lambda_{\text{exc}} = 345$ (ii) 365 and (iii) 385 nm; (b) aqueous dispersion of **P3** (i) $\lambda_{\text{exc}} = 320$ nm, (ii) 340 and (iii) 380 nm.

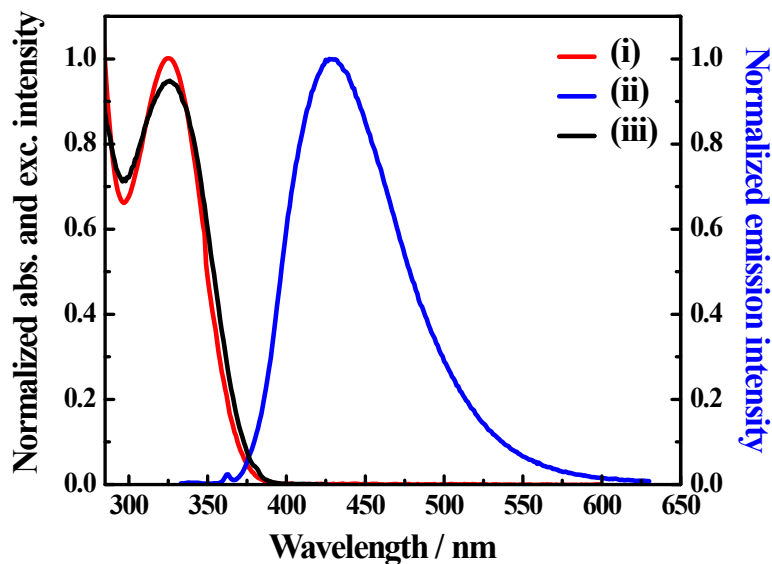


Fig. S15. (i) Absorption, (ii) emission ($\lambda_{\text{exc}} = 326$ nm) and (iii) excitation spectra ($\lambda_{\text{em}} = 427$ nm) of TPDC.

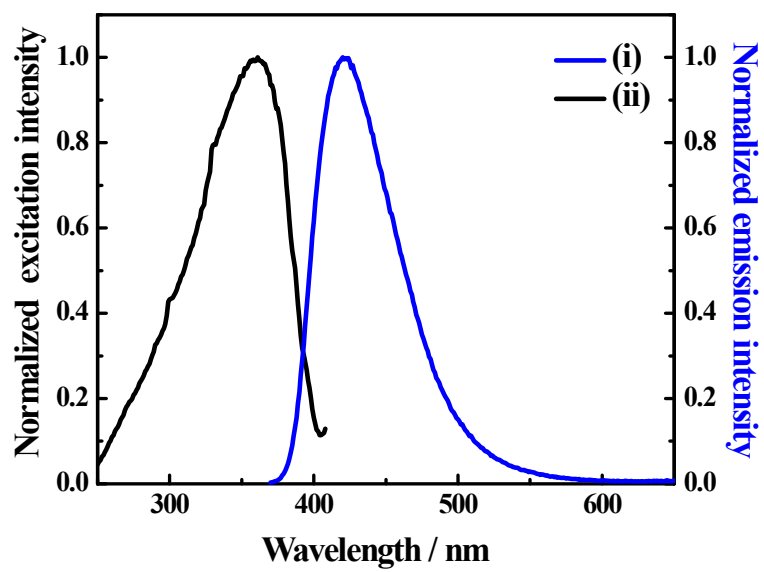


Fig. S16. (i) Emission ($\lambda_{\text{exc}} = 360$ nm) and (ii) excitation spectra ($\lambda_{\text{em}} = 425$ nm) of TBDC in the solid state.

(b) Time-resolved fluorescence measurements

Time-resolved fluorescence measurements were carried out using time-correlated single-photon counting (TCSPC) spectrometer (Delta Flex-01-DD/HORIBA). Delta diode laser 370 nm with FWHM = 154 ps was used as excitation source. Picosecond photon detection module with photomultiplier tube was used as detector. Instrument response function was recorded by using aqueous solution of Ludox. Decay curves were analyzed by nonlinear least-squares iteration using IBH DAS6 (version 6.8) decay analysis software. THF solution of **P2** and nanoparticle dispersion **P3** exhibit average lifetime of 0.94 ns and 0.68 ns respectively.

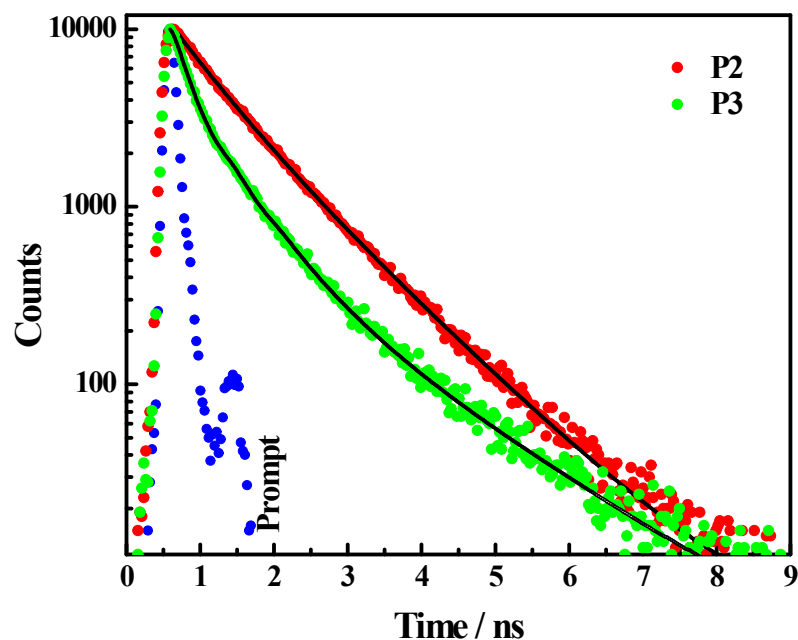


Fig. S17. Fluorescence decay profiles ($\lambda_{\text{exc}} = 370 \text{ nm}$, $\lambda_{\text{em}} = 470 \text{ nm}$) of **P2** in THF and nanoparticles **P3** in water. The continuous black lines are the exponential fit to the decay curves.

Sample	τ_1 (ns)	α_1	τ_2 (ns)	α_2	τ_3 (ns)	α_3	τ_{avg} (ns)	χ^2
P2	0.61	0.36	1.12	0.64	---	---	0.94	1.04

P3	0.18	0.31	0.66	0.50	1.57	0.19	0.68	1.03
-----------	------	------	------	------	------	------	------	------

Table S3. Fluorescence decay parameters for **P2** in THF and nanoparticle **P3** in water; the lifetimes (τ_1 , τ_2 , and τ_3) and the respective fractional contributions (α_1 , α_2 and α_3), the weighted average lifetime (τ_{avg}) and the quality of fitting (χ^2) for the data in Fig. S17 are shown.

VI. Explosive sensing

Both **P2** and **P3** were found to be very effective chemosensors for the detection of nitroaromatic compounds (NC). THF solution of **P2** and as prepared aqueous dispersion of **P3** in presence of surfactants were used for these investigations. The quenching study revealed the gradual decrease of fluorescence intensity on successive addition of NC. Stern-Volmer plots of I_0/I (I_0 and I are the fluorescence intensities in the absence and presence of NC respectively) against $[\text{NC}]$ in THF and water for **P2** and **P3** respectively, show upward bending at higher concentration of NC. To investigate the upward bending in Stern-Volmer plots detailed lifetime measurements were carried out. It was found no significant change in lifetime (Table S4 and S5), which indicates that quenching goes through a static process.⁹ This static quenching phenomenon can be explained by ground state dark fluorophore-quencher complex model (eqn. 1) or effective quencher sphere model (eqn. 2):

$$\frac{I_0}{I} = K_s[\text{NC}] + 1 \quad (1)$$

$$\frac{I_0}{I} = e^{V[\text{NC}]} \quad (2)$$

where, K_s and V are the static quenching constants in the complex and sphere model respectively.⁹ Notably, the eqn. (1) represents that the static quenching is a linear function of $[\text{NC}]$ whereas eqn. (2) represents the same as a nonlinear function of $[\text{NC}]$. Additionally, eqn. (1) can be viewed as an approximation of eqn. (2) when $[\text{NC}]$ and K_s or V are very small. Considering the experimental data eqn. (2) was found to be more suitable. Accordingly, considering picric acid as nitroaromatic analyte, fitting the Stern-Volmer plots of **P2** and **P3** as shown in Fig. 5c and d in the main text eqn. (3) and (4) are obtained respectively.

$$\frac{I_0}{I} = 1.04 e^{2033[\text{PA}]} - 0.04 \quad (3)$$

Fig. S18. Plot of I_0/I against $e^{k[PA]}$: (a) **P2** in THF and (b) aqueous dispersion of nanoparticles **P3**.

Table S4. Fluorescence decay parameters of **P2** in THF upon successive addition of PA.

S.N	[PA]/ 10^{-4} M	τ_1 (ns)	α_1	τ_2 (ns)	α_2	τ_{avg} (ns)
1	1.12	0.47	0.20	1.05	0.80	0.93
2	2.25	0.57	0.31	1.09	0.69	0.93
3	3.37	0.55	0.21	1.03	0.79	0.93
4	4.49	0.47	0.30	1.07	0.70	0.89
5	5.60	0.61	0.36	1.11	0.64	0.93
6	6.67	0.52	0.27	1.06	0.73	0.91
7	7.82	0.44	0.25	1.04	0.75	0.89
8	8.93	0.62	0.40	1.12	0.60	0.92
9	10	0.57	0.31	1.07	0.69	0.91
10	11.1	0.47	0.21	1.02	0.79	0.90
11	12.2	0.54	0.29	1.05	0.71	0.90
12	13.3	0.47	0.22	1.03	0.78	0.90
13	14.4	0.51	0.30	1.05	0.70	0.89
14	15.5	0.48	0.27	1.03	0.73	0.88

15	16.5	0.40	0.24	1.01	0.76	0.86
16	17.6	0.39	0.23	1.00	0.77	0.86

Table S5. Fluorescence decay parameters of **P3** in water upon successive addition of PA.

S.N	[PA]/ 10 ⁻⁶ M	τ_1 (ns)	α_1	τ_2 (ns)	α_2	τ_3 (ns)	α_3	τ_{avg} (ns)
1	2.03	0.59	0.51	0.14	0.27	1.54	0.22	0.68
2	6.09	0.62	0.49	0.17	0.28	1.47	0.23	0.69
3	16.2	0.61	0.53	0.17	0.27	1.60	0.20	0.69
4	30	0.56	0.50	0.14	0.26	1.45	0.24	0.66
5	40	0.54	0.51	0.12	0.24	1.42	0.25	0.66
6	50.4	0.60	0.49	0.19	0.28	1.48	0.23	0.69
7	60.4	0.61	0.53	0.17	0.27	1.59	0.20	0.69
8	70.3	0.59	0.50	0.18	0.27	1.48	0.23	0.68
9	80	0.51	0.48	0.12	0.23	1.34	0.28	0.65
10	90	0.58	0.48	0.17	0.27	1.42	0.25	0.68
11	100	0.53	0.44	0.15	0.26	1.29	0.30	0.66
12	119	0.54	0.49	0.11	0.25	1.40	0.26	0.66
13	139	0.56	0.49	0.12	0.26	1.39	0.25	0.66
14	158	0.48	0.46	0.10	0.23	1.29	0.31	0.64
15	177	0.59	0.47	0.13	0.26	1.35	0.27	0.68
16	196	0.48	0.47	0.11	0.22	1.29	0.31	0.65
17	215	0.45	0.43	0.09	0.21	1.19	0.36	0.64
18	255	0.51	0.49	0.10	0.24	1.37	0.27	0.64
19	263	0.55	0.50	0.17	0.25	1.42	0.25	0.67

20	271	0.53	0.49	0.12	0.24	1.34	0.27	0.65
21	290	0.57	0.49	0.14	0.27	1.42	0.24	0.66
22	308	0.59	0.52	0.19	0.27	1.51	0.21	0.67

Investigation with other nitroaromatics

Apart from picric acid (PA), 2,4-dinitrotoluene (DNT), *m*-dinitrobenzene (DNB) and nitrobenzene (NB) were used as electron deficient nitroaromatic analytes to explore the sensing capabilities of **P2** and **P3**. The mechanism of the quenching process was found to be similar as discussed earlier for PA. The quenching efficiency of nitroaromatic compounds towards **P2** and **P3** was found to follow the order NB < DNB < DNT < PA, consistent with the trend reported earlier for other covalent organic polymers (Table S6 and S7).¹¹ Steady state and time resolved fluorescence studies and Stern-Volmer analysis of fluorescence quenching of **P2** and **P3** by DNT, DNB and NB are presented in figures S19-S24.

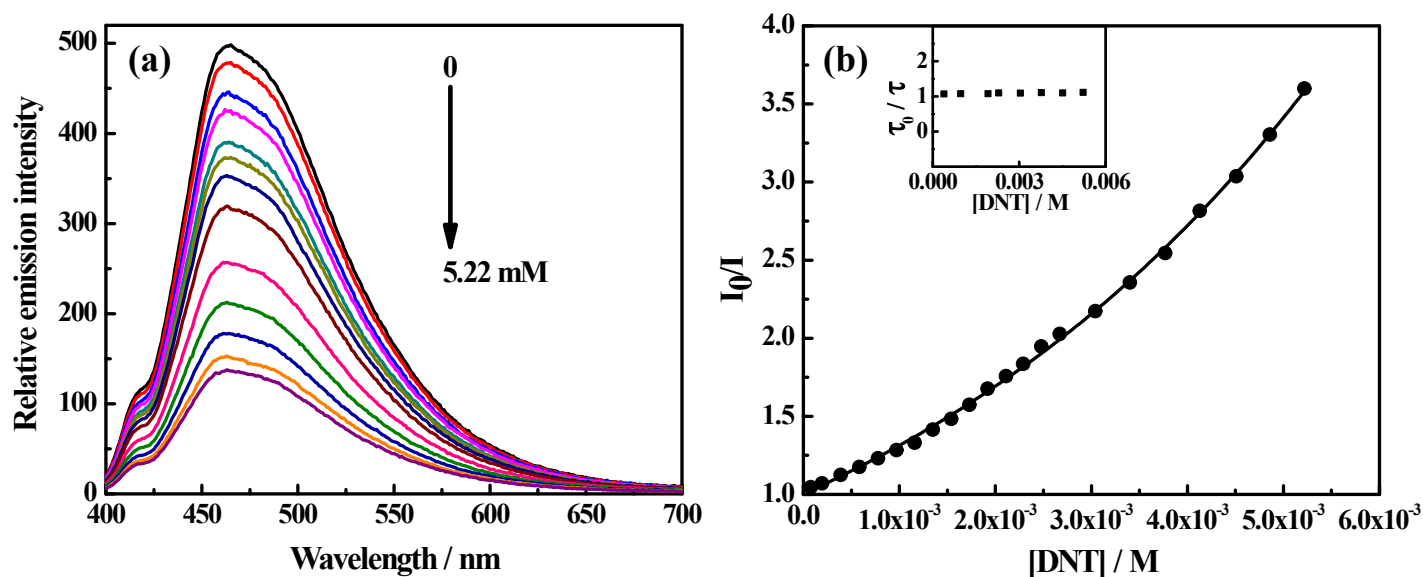


Fig. S19. (a) Emission spectra demonstrating the quenching of fluorescence of **P2** in THF ($\lambda_{\text{exc}} = 365 \text{ nm}$) with increasing concentrations of DNT. (b) Stern-Volmer plots of I_0/I against concentration of DNT ($I_0 =$ fluorescence intensity at $[\text{DNT}] = 0 \text{ M}$); the inset graph refers to plot of corresponding relative fluorescence lifetime (τ_0/τ) against various concentrations of DNT ($\tau_0 =$ lifetime of polymer in absence of DNT).

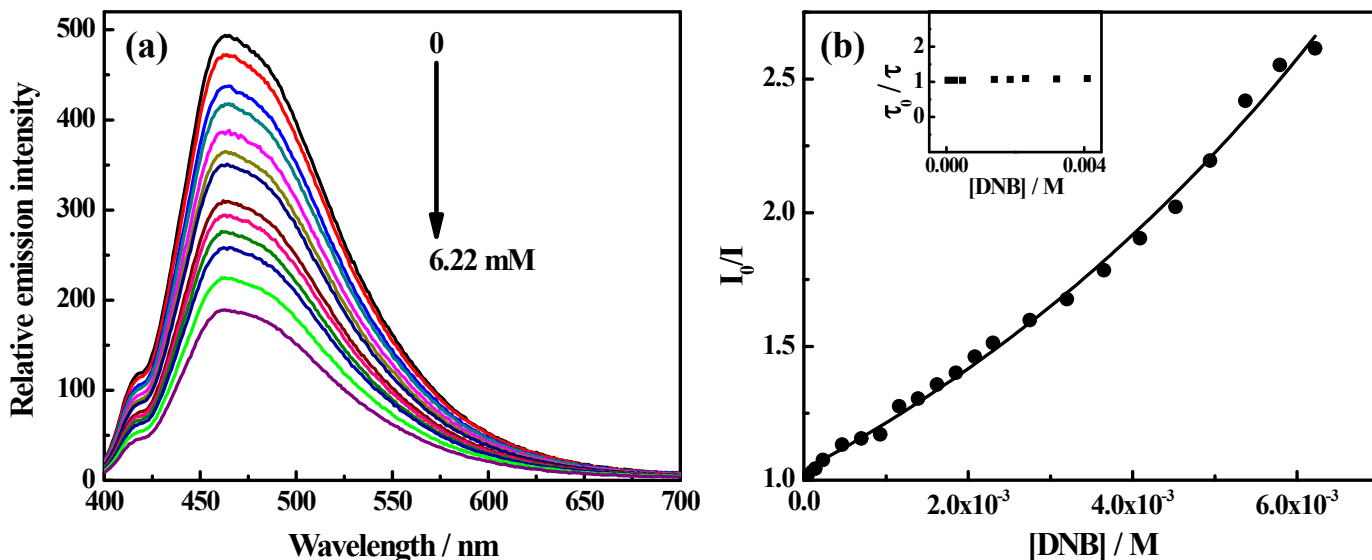


Fig. S20. (a) Emission spectra demonstrating the quenching of fluorescence of **P2** in THF ($\lambda_{exc} = 365$ nm) with increasing concentrations of DNB. (b) Stern-Volmer plots of I_0/I against concentration of DNB (I_0 = fluorescence intensity at $[DNB] = 0$ M); the inset graph refers to plot of corresponding relative fluorescence lifetime (τ_0/τ) against various concentrations of DNB (τ_0 = lifetime of polymer in absence of DNB).

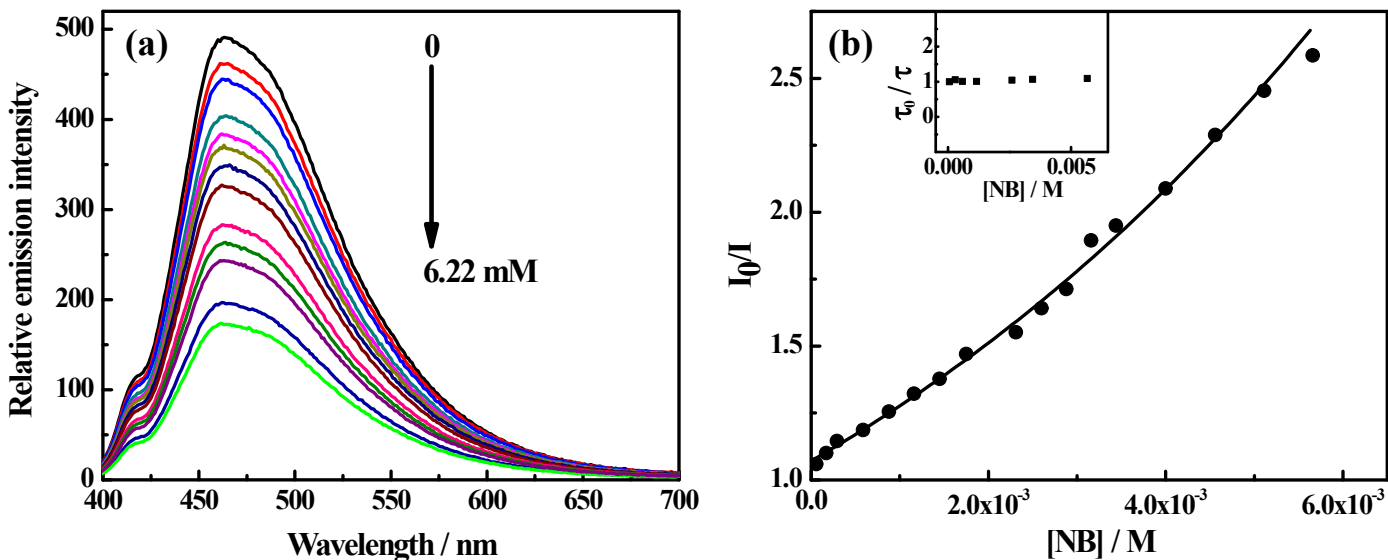


Fig. S21. (a) Emission spectra demonstrating the quenching of fluorescence of **P2** in THF ($\lambda_{exc} = 365$ nm) with increasing concentrations of NB. (b) Stern-Volmer plots of I_0/I against concentration of NB (I_0 = fluorescence intensity at $[NB] = 0$ M); the inset graph refers to plot of corresponding relative fluorescence lifetime (τ_0/τ) against various concentrations of NB (τ_0 = lifetime of polymer in absence of NB).

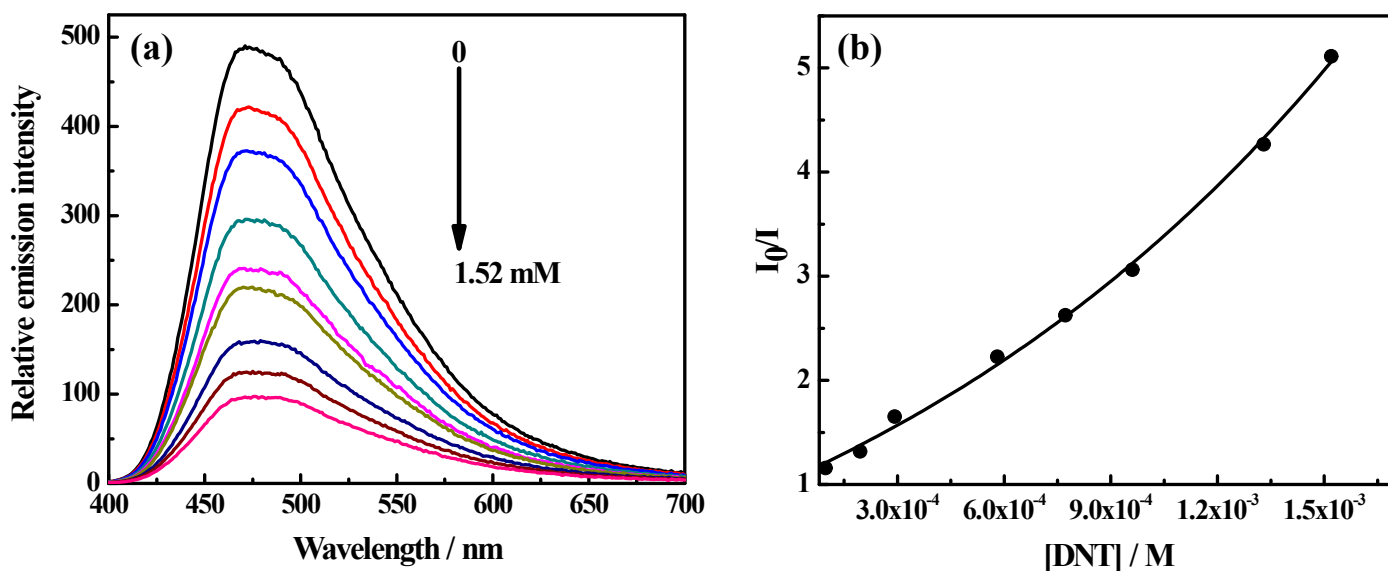


Fig. S22. (a) Emission spectra demonstrating the quenching of fluorescence of **P3** in water ($\lambda_{exc} = 340$ nm) with increasing concentrations of DNT. (b) Stern-Volmer plots of I_0/I against concentration of DNT (I_0 = fluorescence intensity at $[DNT] = 0$ M).

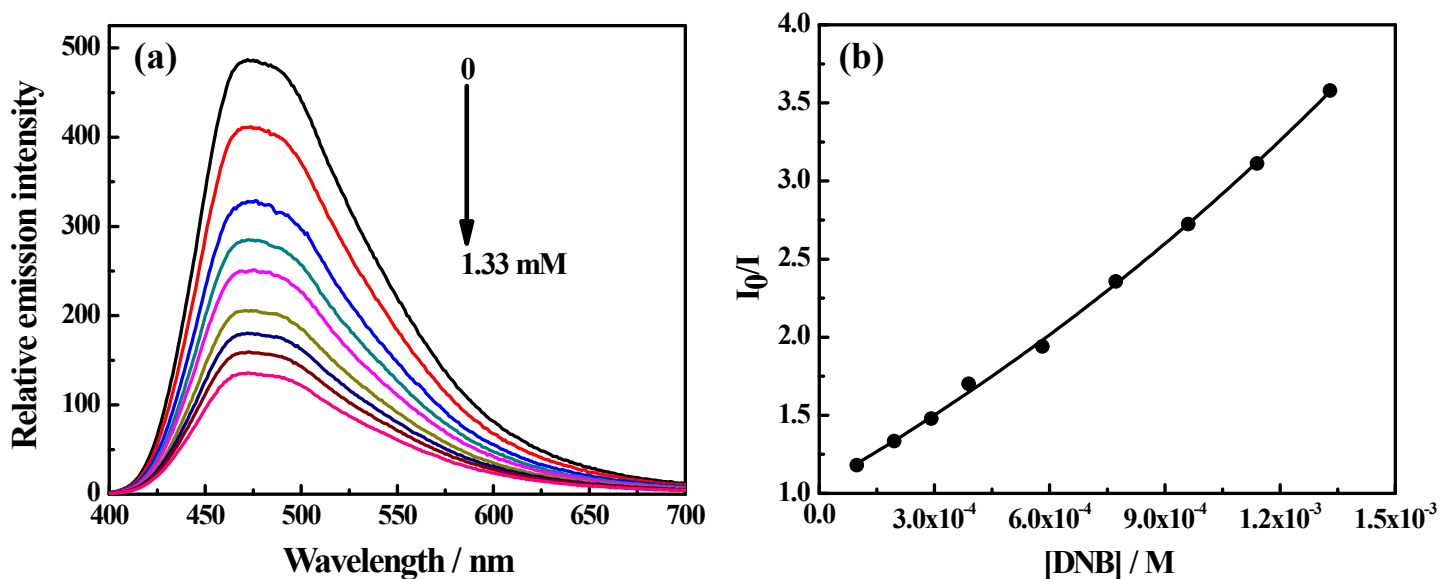


Fig. S23. (a) Emission spectra demonstrating the quenching of fluorescence of **P3** in water ($\lambda_{exc} = 340$ nm) with increasing concentrations of DNB. (b) Stern-Volmer plots of I_0/I against concentration of DNB (I_0 = fluorescence intensity at $[DNB] = 0$ M).

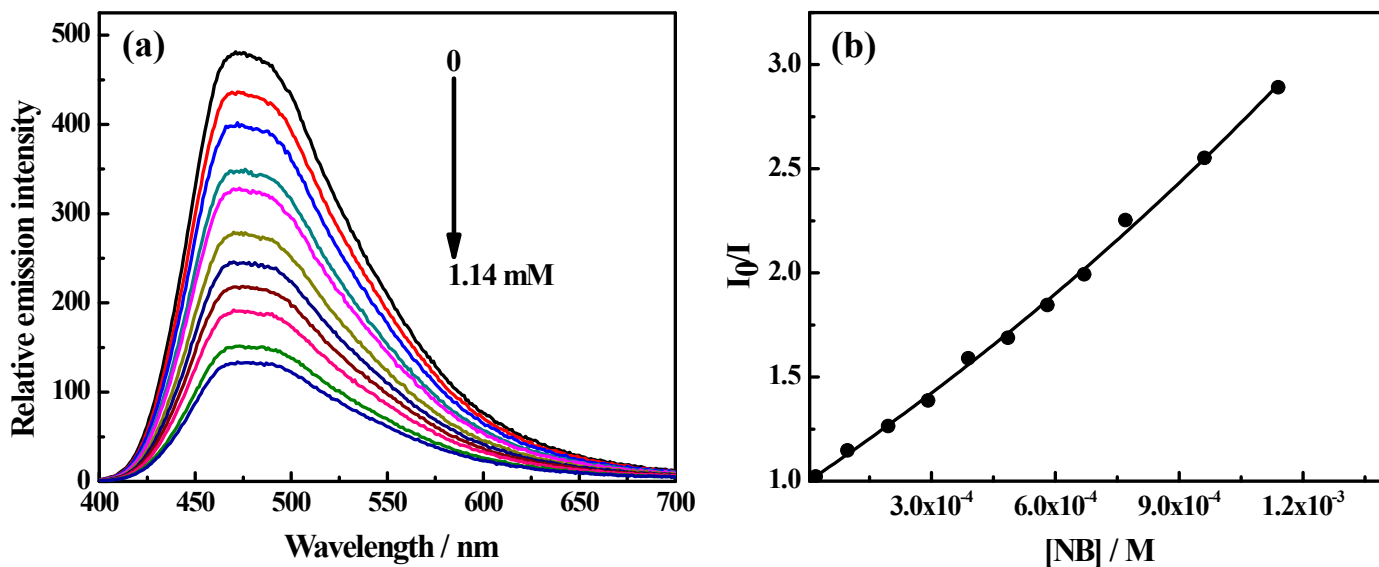


Fig. S24. (a) Emission spectra demonstrating the quenching of fluorescence of **P3** in water ($\lambda_{\text{exc}} = 340 \text{ nm}$) with increasing concentrations of NB. (b) Stern-Volmer plots of I_0/I against concentration of NB ($I_0 =$ fluorescence intensity at $[\text{NB}] = 0 \text{ M}$).

Table S6. A comparative account of explosive quenching by TPDC polymers (**P2** & **P3**).

Polymers	Quenching constant ($K, \text{L mol}^{-1}$) towards different nitroaromatic compounds			
	Picric acid (PA)	2,4-dinitrotoluene (DNT)	<i>m</i> -dinitrobenzene (DNB)	Nitrobenzene (NB)
P2	2.11×10^3	2.79×10^2	1.81×10^2	1.72×10^2
P3	7.62×10^4	1.56×10^3	1.42×10^3	1.34×10^3

The static quenching constants of TPDC based porous organic polymers **P2** ($K = 2.1 \times 10^3 \text{ L mol}^{-1}$) and **P3** ($K = 7.6 \times 10^4 \text{ L mol}^{-1}$) for picric acid detection are much higher compared to reported linear conjugated polymers. A brief comparative account of the explosive detection by fluorescent conjugated polymers is depicted in table S7. Quenching constants are found to be much higher for porous and hyperbranched polymers and their nanoaggregates compared to those of isolated linear conjugated polymers (entry 7). The higher efficiency in porous and branched polymers is associated with the efficient exciton migration.¹⁰

Table S7. A comparative account of explosive quenching by fluorescent conjugated polymers.

No	Type of polymers	Quenching constant (L mol ⁻¹)	Analyte	Source
1	Hyperbranched poly(silylenephenylene)	1.4×10^5	PA	Ref. 10
2	Triphenyl benzene & triphenyl triazine based covalent organic polymers	1.4×10^4 & 3.9×10^3	PA	Ref. 11
		829 & 745	DNT	Ref. 11
		470 & 293	DNB	Ref. 11
		270 & 282	NB	Ref. 11
3	Triphenyl benzene & triphenyl triazine based covalent organic polymers	2.6×10^5 & 8.3×10^4	PA	Ref. 12
4	Carbazole based conjugated microporous polymers	7.2×10^3	DNT	Ref. 13
5	Carbazole based conjugated polymer nanoparticles	1.2×10^6	TNB	Ref. 14
6	Polysiloles	2.0×10^4	PA	Ref. 15
7	Iptycene containing linear conjugated polymers	185	PA	Ref. 16
8	Tetraphenylmetalole dianion based polymers	1.1×10^4	PA	Ref. 17

VII. Tunable emission

Rhodamine 6G (RG) coated **P3** dispersion was prepared by mixing a dilute dispersion of surfactant-stabilized nanoparticles and aqueous solution of the dye. Afterwards, excess dye was removed from the dispersion by dialysis against water using a semi-permeable dialysis membrane. Preliminary exploration indicated that excitation at any wavelength in the absorption band of **P3** nanoparticles in **P3-RG** dispersion resulted in significant quenching of fluorescence from polymer nanoparticles, possibly due to energy transfer from nanoparticles to surface bound Rhodamine 6G dye molecules.

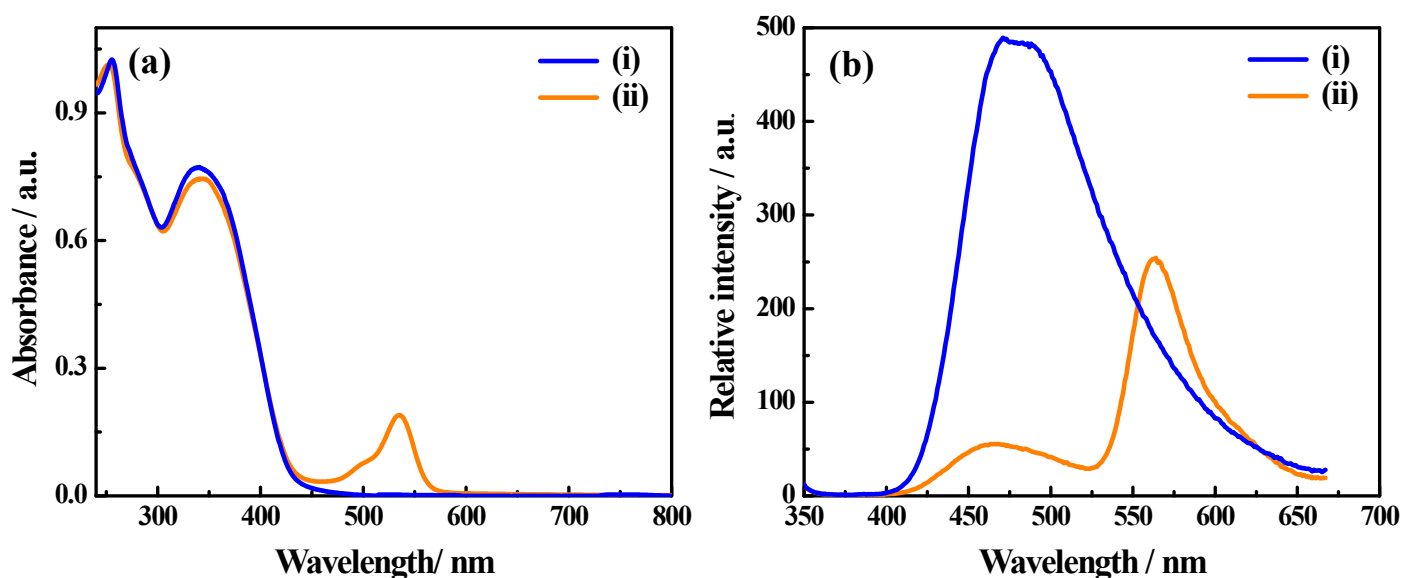


Fig. S25. (a) Absorption spectra of (i) **P3** (ii) **P3-RG** and (b) emission spectra of (i) **P3** (ii) **P3-RG** dispersion ($\lambda_{\text{exc}} = 340$ nm).

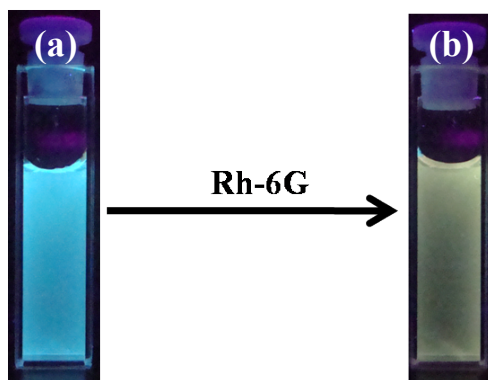


Fig. S26. Photographs of aqueous dispersion of (a) **P3** nanoparticles and (b) that of loaded with Rhodamine 6G.

References

1. L. J. Abbott and C. M. Colina, *Macromolecules*, 2011, **44**, 4511.
2. J. X. Jiang, F. Su, A. Trewin, C. D. Wood, H. Niu, J. T. A. Jones, Y. Z. Khimyak, and A. I. Cooper, *J. Am. Chem. Soc.*, 2008, **130**, 7710.
3. A. Trewin, D. J. Willock and A. I. Cooper, *J. Phys. Chem. C*, 2008, **112**, 20549.
4. L. J. Abbott, A. G. McDermott, A. D. Regno, R. G. D. Taylor, C. G. Bezzu, K. J. Msayib, N. B. McKeown, F. R. Siperstein, J. Runt and C. M. Colina, *J. Phys. Chem. B*, 2013, **117**, 355.
5. L. J. Abbott, K. E. Hart and C. M. Colina, *Theor. Chem. Acc.*, 2013, **132**, 1334.
6. S. Jiang, K. E. Jelfs, D. Holden, T. Hasell, S. Y. Chong, M. Haranczyk, A. Trewin and A. I. Cooper, *J. Am. Chem. Soc.*, 2013, **135**, 17818.
7. C. Wurth, M. Grabolle, J. Pauli, M. Spieles, U.R. Genger, *Nature Protocol.*, 2013, **8**, 1535.
8. K. Rurak, M. Spieles, *Analytical Chem.*, 2011, **83**, 1232.
9. J. R. Lakowicz, *Principles of Fluorescence Spectroscopy*, Springer, New York, 2006.
10. J. Liu, Y. Zhong, P. Lu, Y. Hong, J. W. Y. Lam, M. Faisal, Y. Yu, K. S. Wong and B. Z. Tang *Polym. Chem.*, 2010, **1**, 426.
11. Z. Xiang and D. Cao, *Macromol. Rapid Commun.*, 2012, **33**, 1184.
12. N. Sang, C. Zhan and D. Cao, *J. Mater. Chem. A*, 2015, **3**, 92.
13. Y. Zhang, S. A, Y. Zou, X. Luo, Z. Li, H. Xia, X. Liu and Y. Mu, *J. Mater. Chem. A*, 2014, **2**, 13422.
14. W. Dong, T. Fei, A. Palma-Cando and U. Scherf, *Polym. Chem.*, 2014, **5**, 4048.
15. J. C. Sanchez, A. G. DiPasquale, A. L. Rheingold and W. C. Trogler, *Chem. Mater.*, 2007, **19**, 6459.
16. D. Zhao and T. M. Swager, *Macromolecules*, 2005, **38**, 9377.
17. H. Sohn, M. J. Sailor, D. Magde and W. C. Trogler, *J. Am. Chem. Soc.*, 2003, **125**, 3821.

^1H , ^{13}C NMR spectra of all final compounds

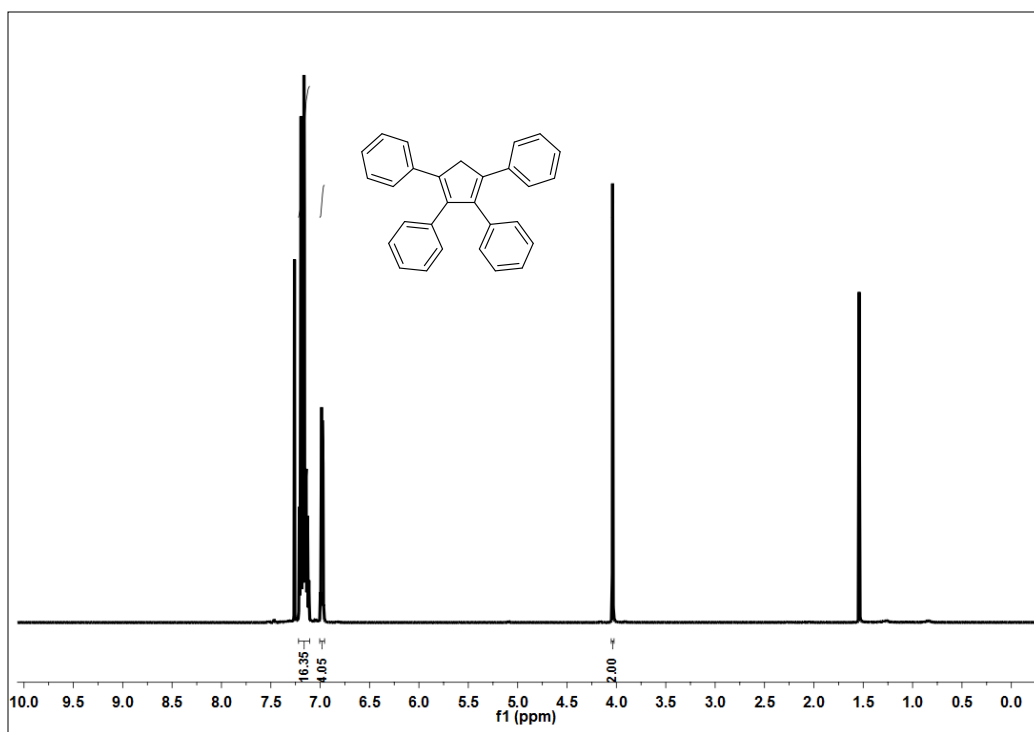


Fig. S27. ^1H NMR spectrum of TPCP.

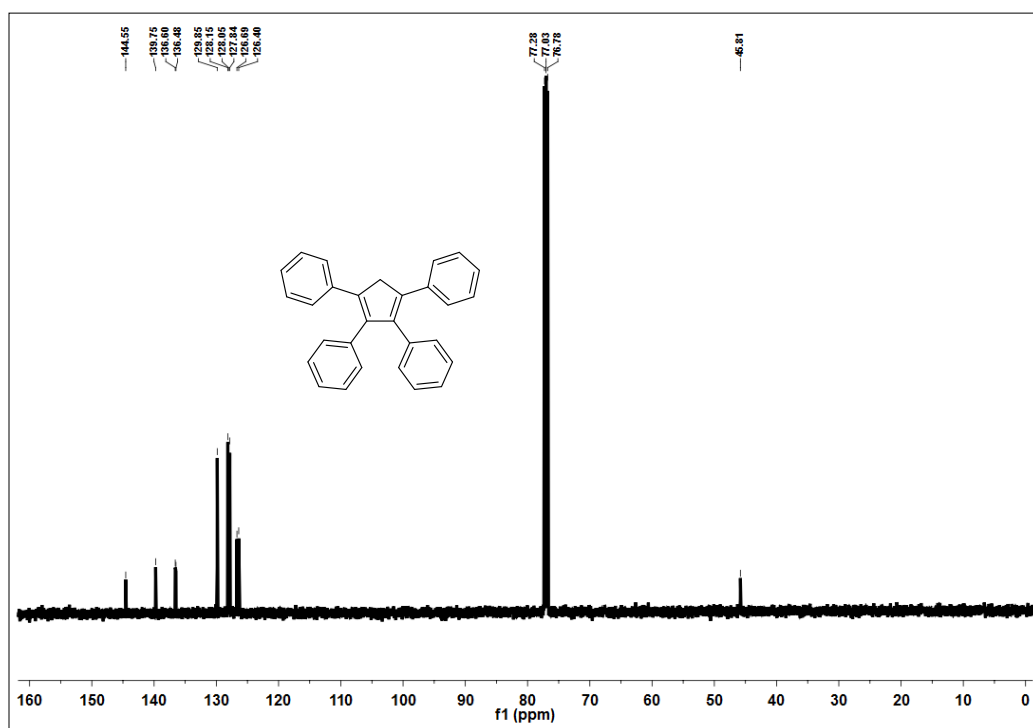


Fig. S28. ^{13}C NMR spectrum of TPCP.

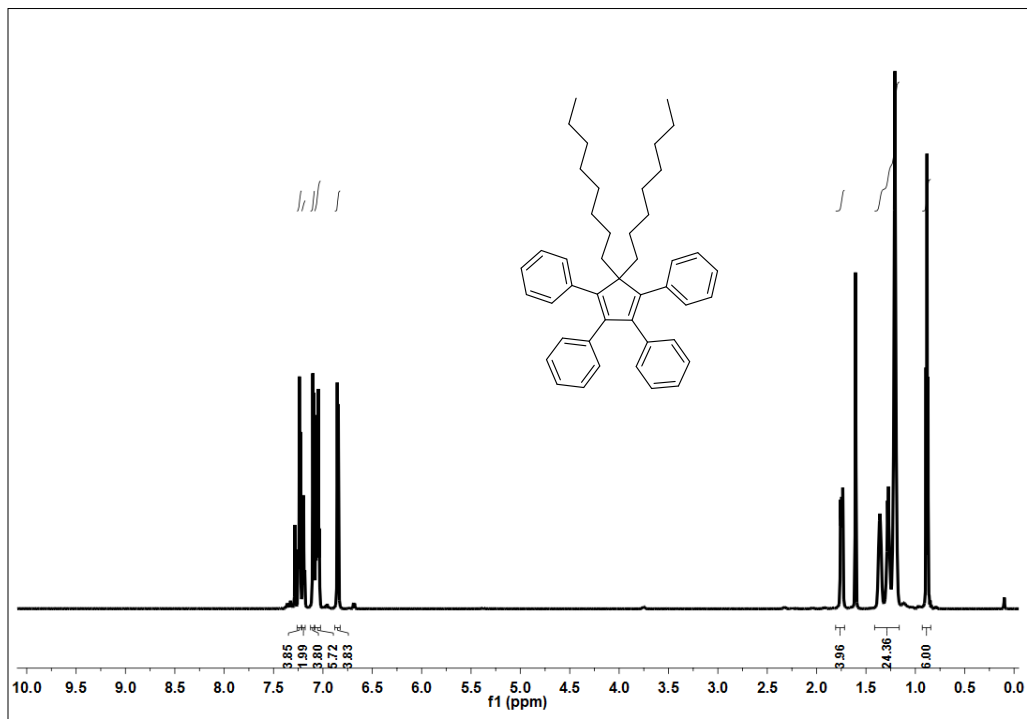


Fig. S29. ¹H NMR spectrum of TPDC.

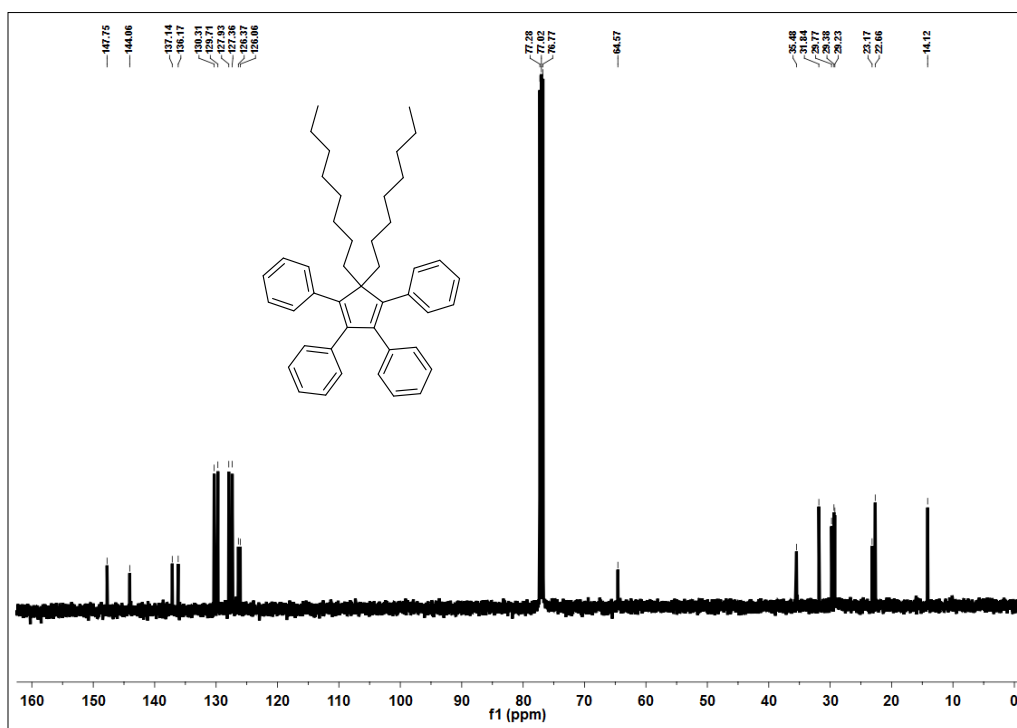


Fig. S30. ¹³C NMR spectrum of TPDC.

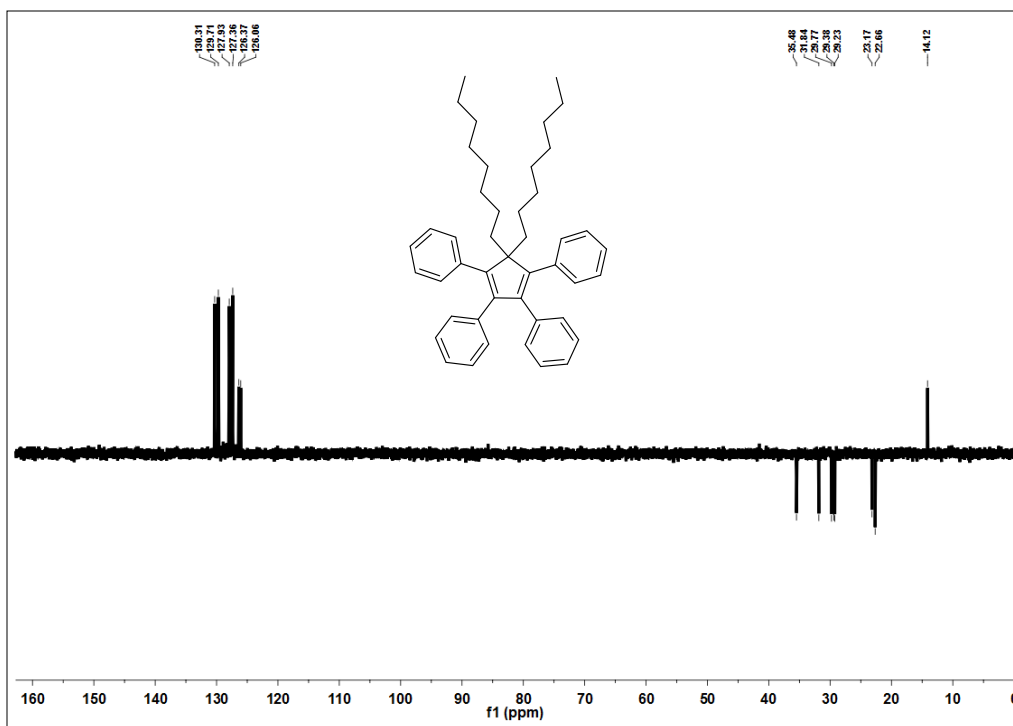


Fig. S31. DEPT-135 spectrum of TPDC.

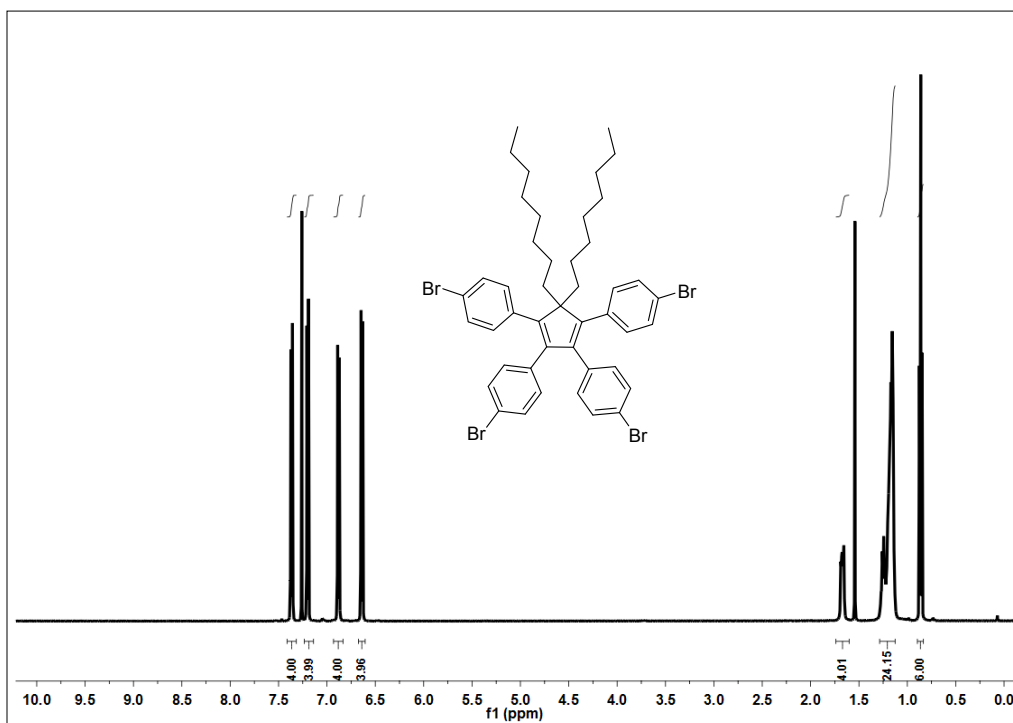


Fig. S32. ^1H NMR spectrum of TBDC.

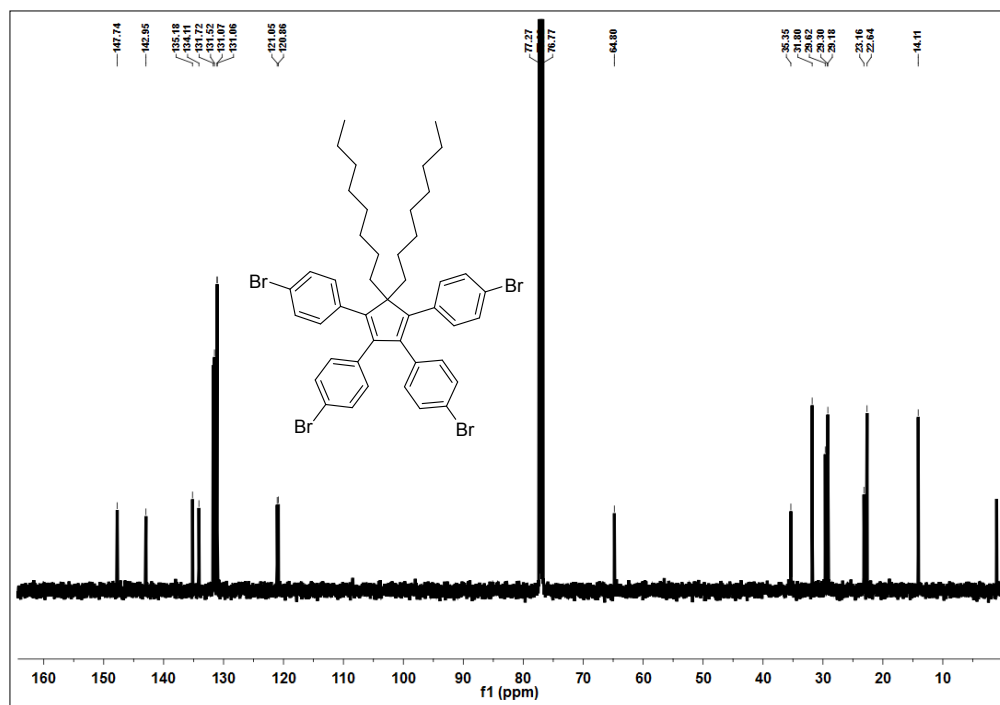


Fig. S33. ^{13}C NMR spectrum of TBDC.

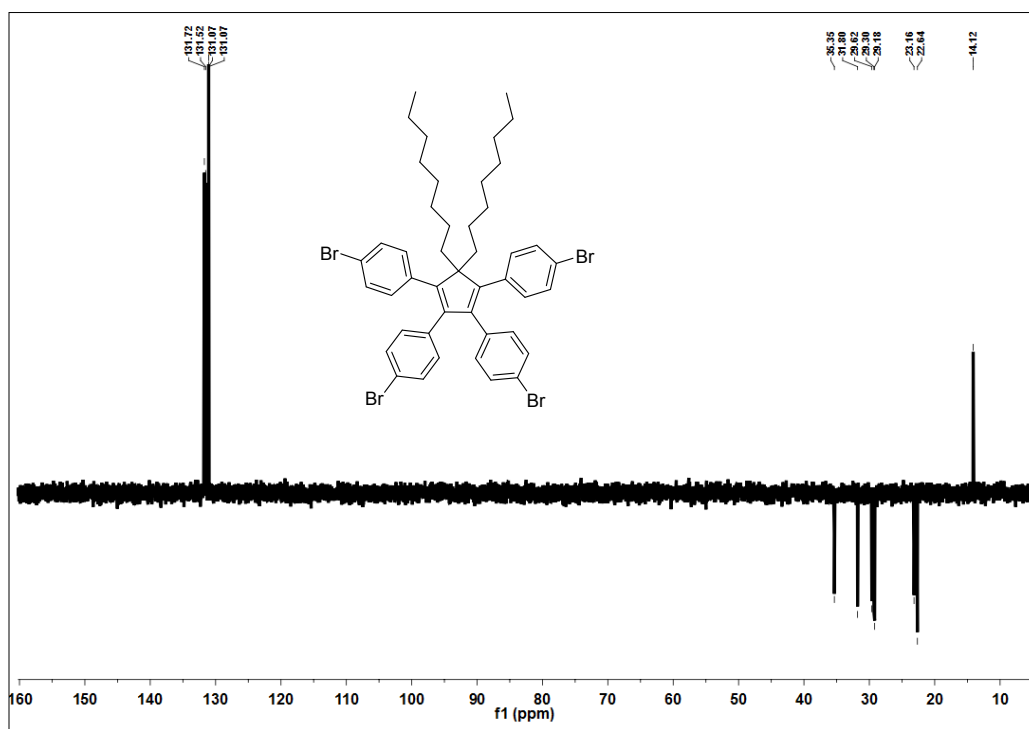


Fig. S34. DEPT-135 spectrum of TBDC.